Spectral Methods - Part 1: A fast and accurate approach for solving nonlinear diffusive problems

Suelen Gasparin, Julien Berger, Denys Dutykh, Nathan Mendes

Suelen Gasparin
Pontifical Catholic University of Paraná, Brazil
LAMA–CNRS, Université Savoie Mont Blanc, France

Julien Berger
LOCIE–CNRS, Université Savoie Mont Blanc, France

Denys Dutykh
LAMA–CNRS, Université Savoie Mont Blanc, France

Nathan Mendes
Pontifical Catholic University of Paraná, Brazil

Spectral Methods — Part 1: A fast and accurate approach for solving nonlinear diffusive problems

arXiv.org / HAL

Last modified: April 24, 2017

Spectral Methods — Part 1: A fast and accurate approach for solving nonlinear diffusive problems

Suelen Gasparin*, Julien Berger, Denys Dutykh, and Nathan Mendes

Abstract. This paper proposes the use of the Spectral method to simulate diffusive moisture transfer through porous materials, which can be strongly nonlinear and can significantly affect sensible and latent heat transfer. An alternative way for computing solutions by considering a separated representation is presented, which can be applied to both linear and nonlinear diffusive problems, considering highly moisture–dependent properties. The Spectral method is compared with the classical implicit Euler and Crank–Nicolson schemes. The results show that the Spectral approach enables to accurately simulate the field of interest. Furthermore, the numerical gains become particularly interesting for nonlinear cases since the proposed method drastically can reduce the computer run time by 99% when compared to the traditional Crank–Nicolson scheme.

Key words and phrases: Spectral methods; numerical simulation of diffusive phenomena; nonlinear problems; Chebyshev polynomials; Galerkin method; moisture diffusion; building physics; reduced–order modelling

MSC: [2010] 35R30 (primary), 35K05, 80A20, 65M32 (secondary)
PACS: [2010] 44.05.+e (primary), 44.10.+i, 02.60.Cb, 02.70.Bf (secondary)

Key words and phrases. Spectral methods; numerical simulation of diffusive phenomena; nonlinear problems; Chebyshev polynomials; Galerkin method; moisture diffusion; building physics; reduced–order modelling.

* Corresponding author.

Contents

1. Introduction

Moisture transfer through porous structures is a matter of concern in many areas such as building physics, food engineering, hydrology, agriculture, geophysics, environmental engineering and energy systems, among others, where the transient evolution of moisture may play a role of paramount importance. Particularly in the area of building physics, moisture transfer process through the porous envelope, roofing systems, ground, and furniture may strongly affect energy and hygrothermal performance of those elements at the same time moisture may impact on indoor air quality and material deterioration.

Models for moisture transfer through porous building materials have been presented in many building simulation tools since the 1990's, in software such as Delphin [5], MATCH [32], MOIST [8], WUFI [14] and UMIDUS [24, 27, 31]. Moisture models have also been implemented in whole–building simulation tools and tested in the frame of the International Energy Agency Annex 41, which reported on most of detailed models and their successful applications for accurate assessment of hygrothermal transfer in buildings [37].

As building material properties are temperature– and moisture–dependent and the boundary conditions are driven by weather variables, the models included in those tools are based on numerical approaches using discrete representations of the continuous equations. To compute the solution, standard discretisation and incremental techniques are applied such as the EULER implicit scheme in [5, 14, 19, 20, 26, 33, 35] to solve large systems of equations (of an order of 10^6 for 3−dimensional problems). Furthermore, when dealing with nonlinearities, hygrothermal properties of porous materials have to be updated as a function of the temperature and moisture content fields at each iteration. The difficulties to compute the solution increase, particularly when using implicit schemes that require sub-iterations to treat those issues. In the literature, the important numerical costs of simulation tools [2, 11, 12, 29] is also mentioned and it is a matter of concern due to the great scale of buildings, where heat and moisture transfer phenomena have to be simulated. Thus, innovative and efficient ways of numerical simulation are worth of further investigation. Model reduction techniques are an alternative approach to deal with this problem.

Model reduction is related to the decrease of the model *order* and, thus, complexity. Sometimes its definition is confused and the concepts are not very clear. In this paper, for the sake of clarity, the term *fidelity* is used to denote the ability of a model to represent the physical phenomenon [22]. Thus, the linear moisture model can be considered as a low fidelity model, compared to a model that considers nonlinear transfer or even the coupled heat and moisture nonlinear transfer phenomena into account. The term Reduced Order Models (ROM) has the purpose of decreasing the degrees of freedom of a numerical model, retaining the model ability to capture the essential physics. In other words, reduced order models aim at providing accurate descriptions of the dynamics but with significantly lower computational costs. Reduced order models intend to identify genuine degrees of freedom and give low–dimensional approximations, preserving a satisfactory accuracy that saves computational resources (CPU time and memory).

Reduced order models can be classified as *a priori* or *a posteriori* methods. The *a posteriori* approaches need a preliminary computed (or even experimental) solution data of the large original problem to build the reduced one. Whereas the *a priori* ones does not need preliminary information on the studied problem. The reduced order model is unknown *a priori* and is directly built. Since the 2000$^{\text{th}}$, aiming to reduce the computational cost, reduction model techniques started to take place in the context of heat and moisture transfer for building physics applications, as an alternative for traditional methods. Different kinds of approaches can be considered, such as the *a posteriori* Proper Orthogonal Decomposition (POD), the Modal Basis Reduction (MBR) and the *a priori* Proper Generalized Decomposition (PGD), which have shown relevant reduction of the computational cost for successful applications in the building physics area [6].

Therefore, this paper aims at presenting an innovative approach, never applied in the context of building physics, *i.e.*, the *a priori* Spectral reduced order model technique to compute the moisture transfer in porous materials. The manuscript is organized as follows. First, the description of the physical phenomena is presented (Section 2). Then, the explanation of the Spectral reduced order model techniques are described (Section 3). In the sequence, an application of ROM techniques to three different cases are shown. The first one considers linear transfer (Section 4.1) to validate the method. The second one focuses on a weak nonlinear transfer (Section 4.2), in which some simplifications are considered, while the last one presents a strongly nonlinear transfer case with moisture–dependent material properties (Section 5).

2. Moisture transfer in porous materials

The physical problem involves one–dimensional moisture diffusion through a porous material defined by the spatial domain $\Omega_x = [0, L]$. The moisture transfer occurs according to liquid and vapour diffusion processes. The physical problem can be formulated as [1, 23]:

$$\frac{\partial \rho_{l+v}}{\partial t} = \frac{\partial}{\partial x}\left(k_l \frac{\partial P_c}{\partial x} + k_v \frac{\partial P_v}{\partial x} \right), \tag{2.1}$$

where ρ_{l+v} is the volumetric moisture content of the material and k_v and k_l, the vapour and liquid permeabilities.

Eq. (2.1) can be written using the vapour pressure P_v as the driving potential. For this, we consider the physical relation, known as the Kelvin equation, between P_v and P_c:

$$\begin{aligned} P_c &= R_v \cdot T \cdot \ln\left(\frac{P_v}{P_s(T)}\right), \\ \frac{\partial P_c}{\partial P_v} &= \frac{R_v T}{P_v}. \end{aligned}$$

Thus, we have:

$$\frac{\partial P_c}{\partial x} \;=\; \frac{\partial P_c}{\partial P_v}\cdot\frac{\partial P_v}{\partial x} \;+\; \frac{\partial P_c}{\partial T}\cdot\frac{\partial T}{\partial x}\,.$$

As we consider mass transfer under isothermal conditions, the second right–hand term vanishes and we obtain:

$$\frac{\partial P_c}{\partial x} \;=\; \frac{R_v\,T}{P_v}\cdot\frac{\partial P_v}{\partial x}\,.$$

In addition, we have:

$$\frac{\partial \rho_{l+v}}{\partial t} \;=\; \frac{\partial \rho_{l+v}}{\partial \phi}\cdot\frac{\partial \phi}{\partial P_v}\cdot\frac{\partial P_v}{\partial t} \;+\; \frac{\partial \rho_{l+v}}{\partial T}\cdot\frac{\partial T}{\partial t} \;\simeq\; \frac{\partial \rho_{l+v}}{\partial \phi}\cdot\frac{\partial \phi}{\partial P_v}\cdot\frac{\partial P_v}{\partial t}\,.$$

Considering the relation $\rho_{l+v} \;=\; f\,(\phi) \;=\; f\,(\,P_v\,,T\,)$, obtained from material properties and from the relation between the vapour pressure P_v and the relative humidity ϕ, we get:

$$\frac{\partial \rho_{l+v}}{\partial t} \;=\; f\,'(P_v)\cdot\frac{1}{P_s}\cdot\frac{\partial P_v}{\partial t}\,.$$

Eq. (2.1) can be therefore rewritten as:

$$f\,'(P_v)\cdot\frac{1}{P_s}\cdot\frac{\partial P_v}{\partial t} \;=\; \frac{\partial}{\partial x}\left[\left(k_l\,\frac{R_v\,T}{P_v} \;+\; k_v\right)\cdot\frac{\partial P_v}{\partial x}\right]. \tag{2.2}$$

The material properties $f\,'(P_v)$, k_l and k_v depend on the vapour pressure P_v. Therefore, we denote $d_m \overset{\text{def}}{:=} k_l\cdot\dfrac{R_v\,T}{P_v} \;+\; k_v$ as the global moisture transport coefficient and $c_m \overset{\text{def}}{:=} f\,'(P_v)\,\dfrac{1}{P_s}$, the moisture storage coefficient.

At the material bounding surfaces, Robin–type boundary conditions are considered:

$$\left(k_l\,\frac{R_v\,T}{P_v} \;+\; k_v\right)\cdot\frac{\partial P_v}{\partial x} \;=\; h_{v,\mathrm{L}}\cdot(\,P_v \;-\; P_{v,\mathrm{L}}\,) \;-\; g_{l,\mathrm{L}}\,, \qquad x \;=\; 0\,, \tag{2.3}$$

$$-\left(k_l\,\frac{R_v\,T}{P_v} \;+\; k_v\right)\cdot\frac{\partial P_v}{\partial x} \;=\; h_{v,\mathrm{R}}\cdot(\,P_v \;-\; P_{v,\mathrm{R}}\,) \;-\; g_{l,\mathrm{R}}\,, \qquad x \;=\; L\,, \tag{2.4}$$

where P_v is the vapour pressure of the ambient air, g_l, the liquid water flow (driving rain), R and L stand for the right and left bounding surfaces.

We consider a uniform vapour pressure distribution as the initial condition:

$$P_v \;=\; P_v^{\,i}\,, \qquad\qquad t \;=\; 0\,. \tag{2.5}$$

It is important to obtain a unitless formulation of governing equations while performing mathematical and numerical analysis of given practical problems, due to certain number

of reasons already discussed in [16]. Therefore, we define the following dimensionless parameters:

$$u = \frac{P_v}{P_v^i}, \qquad u_{\mathrm{R}} = \frac{P_{v,\mathrm{R}}}{P_v^i}, \qquad u_{\mathrm{L}} = \frac{P_{v,\mathrm{L}}}{P_v^i}, \qquad x^\star = \frac{x}{L},$$

$$t^\star = \frac{t}{t^0}, \qquad c_m^\star = \frac{c_m \cdot L^2}{d_m^0 \cdot t^0}, \qquad d_m^\star = \frac{d_m}{d_m^0}, \qquad \mathrm{Bi}_{v,\mathrm{L}} = \frac{h_{v,\mathrm{L}} \cdot L}{d_m^0},$$

$$\mathrm{Bi}_{v,\mathrm{R}} = \frac{h_{v,\mathrm{R}} \cdot L}{d_m^0}, \qquad g_{l,\mathrm{L}}^\star = \frac{g_{l,\mathrm{L}} \cdot L}{d_m^0 \cdot P_v^i}, \qquad g_{l,\mathrm{R}}^\star = \frac{g_{l,\mathrm{R}} \cdot L}{d_m^0 \cdot P_v^i}.$$

In this way, the dimensionless governing equations can then be written as:

$$c_m^\star \frac{\partial u}{\partial t^\star} = \frac{\partial}{\partial x^\star}\left(d_m^\star \frac{\partial u}{\partial x^\star} \right), \qquad t^\star > 0, \qquad x^\star \in \left[0, 1\right], \tag{2.6a}$$

$$d_m^\star \frac{\partial u}{\partial x^\star} = \mathrm{Bi}_{v,\mathrm{L}} \cdot (u - u_{\mathrm{L}}) - g_{l,\mathrm{L}}^\star, \qquad t^\star > 0, \qquad x^\star = 0, \tag{2.6b}$$

$$-d_m^\star \frac{\partial u}{\partial x^\star} = \mathrm{Bi}_{v,\mathrm{R}} \cdot (u - u_{\mathrm{R}}) - g_{l,\mathrm{R}}^\star, \qquad t^\star > 0, \qquad x^\star = 1, \tag{2.6c}$$

$$u = 1, \qquad t^\star = 0, \qquad x^\star \in \left[0, 1\right]. \tag{2.6d}$$

Finally, this is the problem of interest considered here for the Spectral reduced order model resolution. Now, the method procedure will be described to propose a reduce order model for the solution of this problem.

3. Reduced Spectral method for linear transfer

While finite–difference and finite–element methods are based on local representation of functions, using low–order approximations, Spectral methods consider a global representation of the solution, which yields beyond all orders approximations [7]. In the global representation approach, the value of the derivative at a certain spatial location depends on the solution on the entire domain and not only on its neighbours. Spectral method considers a sum of Spectral modes that suits for the whole domain, almost like an analytical solution, providing a global approximation with very few modes, as it will be demonstrated below. For smooth solutions, its error decreases exponentially when the number of modes is increases, $\mathcal{O}(\mathrm{e}^{-cN})$. Thus, it is possible to have the same accuracy of other methods but with a much lower number of collocation points, which makes this method memory usage minimized, allowing to store and operate a lower number of degrees of freedom [36].

3.1. Method description

For the sake of simplicity and without loosing the generality, this method is first explained considering the dimensionless coefficients $d_m^\star$ and $c_m^\star$ as constants, noting $\nu \overset{\text{def}}{:=} \frac{d_m^\star}{c_m^\star}$

and thus, considering the linear diffusion equation:

$$\frac{\partial u}{\partial t} \;=\; \nu \frac{\partial^2 u}{\partial x^2}\,, \tag{3.1}$$

for $t > 0$ and $x \in \left[-1, 1\right]$. A special attention must be given to the spatial domain, because the Chebyshev Spectral method we use is described between the interval $\left[-1, 1\right]$. Thus, if the dimensionless interval is not in this interval, a change of variables (domain transformation) must be performed for the computational domain.

The boundary conditions are written as:

$$\frac{\partial u}{\partial x} \;=\; \mathrm{Bi}_{v,\mathrm{L}} \cdot \Big(u - u_{\mathrm{L}}\big(t\big)\Big)\,, \qquad x \;=\; -1\,, \tag{3.2a}$$

$$-\frac{\partial u}{\partial x} \;=\; \mathrm{Bi}_{v,\mathrm{R}} \cdot \Big(u - u_{\mathrm{R}}\big(t\big)\Big)\,, \qquad x \;=\; 1\,. \tag{3.2b}$$

The Spectral method assumes that the unknown $u(x,t)$ from Eq. (3.1) can be approximatively represented as a finite sum [25, Chapter 6]:

$$u\,(x,\,t) \;\approx\; u_n\,(x,\,t) \;=\; \sum_{i\,=\,0}^{n} a_i\,(t)\,\phi_i\,(x)\,. \tag{3.3}$$

Here, $\{\phi_i(x)\}_{i=0}^{n}$ is a set of basis functions that remains constant in time, $\{a_i(t)\}_{i=0}^{n}$ are the corresponding time–dependent Spectral coefficients, n represents the number of degrees of freedom of the solution. Eq. (3.3) can be seen as a series truncation after $N = n + 1$ modes. The Chebyshev polynomials are chosen as the basis functions as they are optimal in $\mathcal{L}_\infty$ approximation norm [17]. It should be observed that other bases can be used, such as the Fourier and Legendre polynomials. Therefore, we have:

$$\phi_i\,(x) \;\equiv\; T_i\,(x)\,.$$

The first Chebyshev polynomials are:

$$T_0\,(x) \;=\; 1\,, \quad T_1\,(x) \;=\; x\,, \quad T_2\,(x) \;=\; 2\,x^2 \;-\; 1\,, \quad T_3\,(x) \;=\; 4\,x^3 \;-\; 3x\,, \ldots$$

and, higher order polynomials can be constructed using a recursive relation [30]:

$$T_{i+1}\,(x) \;=\; 2\,x\,T_i\,(x) \;-\; T_{i-1}\,(x)\,.$$

As we have chosen the basis functions, now we can write the derivatives:

$$\frac{\partial u_n}{\partial x} \;=\; \sum_{i\,=\,0}^{n} a_i\,(t)\,\frac{\partial T_i}{\partial x}\,(x) \;=\; \sum_{i\,=\,0}^{n} \tilde{a}_i\,(t)\,T_i\,(x)\,, \tag{3.4a}$$

$$\frac{\partial^2 u_n}{\partial x^2} \;=\; \sum_{i\,=\,0}^{n} a_i\,(t)\,\frac{\partial^2 T_i}{\partial x^2}\,(x) \;=\; \sum_{i\,=\,0}^{n} \tilde{\tilde{a}}_i\,(t)\,T_i\,(x)\,, \tag{3.4b}$$

$$\frac{\partial u_n}{\partial t} \;=\; \sum_{i\,=\,0}^{n} \dot{a}_i\,(t)\,T_i\,(x)\,, \tag{3.4c}$$

where the dot denotes $\dot{a}_i(t) \overset{\text{def}}{:=} \dfrac{\mathrm{d}a}{\mathrm{d}t}$. Note that the derivatives are written in a such way the Chebyshev polynomials remain the same. As a result, coefficients $\{\tilde{a}_i(t)\}$ and $\{\tilde{\tilde{a}}_i(t)\}$ must be re–expressed in terms of coefficients $\{a_i(t)\}$. The connection is given explicitly from the recurrence relation of the Chebyshev polynomial derivatives [30]:

$$\tilde{a}_i \;=\; \frac{2}{c_i} \sum_{\substack{p=i+1 \\ p+i \text{ odd}}}^{n} p\, a_p\,, \qquad\qquad i \;=\; 0, \ldots, n-1, \tag{3.5a}$$

$$\tilde{\tilde{a}}_i \;=\; \frac{1}{c_i} \sum_{\substack{p=i+2 \\ p+i \text{ even}}}^{n} p\,(p^2 \;-\; i^2)\, a_p\,, \qquad\qquad i \;=\; 0, \ldots, n-2, \tag{3.5b}$$

with,

$$c_i \;=\; \begin{cases} 2 & \text{if} \quad i \;=\; 0\,, \\ 1 & \text{if} \quad i \;>\; 0\,. \end{cases}$$

Replacing the derivative Eq. (3.4a) into the boundary conditions Eq. (3.2), we get:

$$\sum_{i=0}^{n} \tilde{a}_i(t)\, T_i(-1) \;-\; \mathrm{Bi}_{v,\mathrm{L}} \sum_{i=0}^{n} a_i(t)\, T_i(-1) \;+\; \mathrm{Bi}_{v,\mathrm{L}}\, u_{\mathrm{L}}(t) \;=\; 0\,, \tag{3.6a}$$

$$-\sum_{i=0}^{n} \tilde{a}_i(t)\, T_i(1) \;-\; \mathrm{Bi}_{v,\mathrm{R}} \sum_{i=0}^{n} a_i(t)\, T_i(1) \;+\; \mathrm{Bi}_{v,\mathrm{R}}\, u_{\mathrm{R}}(t) \;=\; 0\,, \tag{3.6b}$$

with $T_i(-1) \;=\; (-1)^i$ and $T_i(1) \;\equiv\; 1$ (see [30]). Proceeding with the substitutions, the derivatives (3.4b) and (3.4c) are replaced in the diffusion equation (3.1), leading to the residual:

$$R \;=\; \left\| \sum_{i=0}^{n} \left[\, \dot{a}_i(t) \;-\; \nu\, \tilde{\tilde{a}}_i(t) \,\right] T_i(x) \right\| \longrightarrow \min\,, \tag{3.7}$$

which is considered a misfit of the approximate solution. By minimizing the residual defined in Eq. (3.7) we require that Spectral coefficients of the residual vanish:

$$\dot{a}_i(t) \;-\; \nu\, \tilde{\tilde{a}}_i(t) \;=\; 0\,, \qquad\qquad i \;=\; 0,\, 1,\, \ldots,\, n-2\,,$$

so that, when expanded and projected, it leads to a system of ordinary differential equations (ODE), with $N-2$ equations to be solved as a function of time. The two extra coefficients are obtained from the boundary conditions, Eqs. (3.6a) and (3.6b), written in a explicit way in terms of other coefficients.

Therefore, the original partial differential equation (3.1) is reduced to a system of ODE plus two algebraic expressions. For linear problems, the ODE system is explicitly built with the help of the software `Maple`®. Moreover, the reduced system of ordinary differential equations has the following form:

$$\dot{a}_i(t) \;=\; \mathcal{A}\, a_i(t) + \mathrm{b}\,(t)\,, \qquad\qquad i \;=\; 0,\, 1,\, \ldots,\, n-2\,, \tag{3.8}$$

where, $\mathcal{A} \in \mathrm{Mat}_{(n-2)\times(n-2)}(\mathbb{R})$, with constant coefficients and with $n \simeq \mathcal{O}(10)$. Besides, $\mathrm{b}(t) \in \mathbb{R}^{(n-2)}$ is a vector coming usually from boundary conditions.

Initial values of the coefficients $\{a_i(t = 0)\}$ are calculated by projecting the initial condition [9]:

$$a_i(0) = \frac{2}{\pi c_i} \int_{-1}^{1} \frac{u_0(x)\, T_i(x)}{\sqrt{1 - x^2}}\, \mathrm{d}x\,, \qquad i = 0, 1, \ldots, n-2\,, \tag{3.9}$$

where, $u_0(x)$ is the dimensionless initial condition. After solving the *reduced* ODE system (Eqs. 3.8 and 3.9), it is possible to compose the solution along with the Chebyshev polynomial.

3.1.1 Reduced model usage

By using the Spectral–ROM approach to build the reduced order model, the time dependent coefficients $\big(a_i(t)\big)$ are computed by solving the following system:

$$\begin{cases} \dot{a} &= \mathcal{A}\, a + \mathrm{b}(t)\,, \\ a(0) &= a_0\,, \end{cases}$$

remembering that $\mathcal{A} \in \mathrm{Mat}_{s\times s}(\mathbb{R})$ as a constant coefficient matrix, $\mathrm{b}(t) \in \mathbb{R}^s$ is a vector coming from the boundary conditions and a_0 is the vector of initial coefficients. The main advantage of a Spectral–ROM is that $s \ll p$, where p is the number of degrees of freedom needed to solve problem (3.2) by means of conventional methods such as finite-difference, finite-volume or finite-element methods. We note that matrix $\mathcal{A}$ and vector $\mathrm{b}(t)$ might depend on problem parameters, such as the diffusion coefficient ν:

$$\mathcal{A} = \mathcal{A}(t\,;\nu)\,, \quad \text{and} \quad \mathrm{b} = \mathrm{b}(t\,;\nu)\,.$$

where the symbol ; denotes the separation between the arguments and the parameters.

The advantage of the Spectral–ROM approach is that there are essentially two approximations: (i) the choice of the Spectral expansion and (ii) the truncation to the N modes. Henceforth, the dependence on parameters is the most accurate within the chosen Spectral framework. Let us consider a more general situation:

$$\begin{cases} \dot{a} &= \mathcal{A}(\nu)\, a + \mathrm{b}(t\,, a(t)\,;\nu)\,, \\ a(t_0) &= a_0\,, \end{cases} \tag{3.10}$$

where $\mathrm{b}(t\,, a(t)\,;\nu)$ depends on the solution $a(t)$ via nonlinear boundary conditions, or it contains problem's nonlinearities, if there are some. The general analytical solution to problem (3.10) can be written as:

$$a(t\,;\nu) = \mathrm{e}^{(t\,-\,t_0)\,\mathcal{A}(\nu)} a_0 + \int_{t_0}^{t} \mathrm{e}^{(t\,-\,\tau)\,\mathcal{A}(\nu)}\, \mathrm{b}\big(\tau\,, a(\tau)\,;\nu\big)\, \mathrm{d}\tau\,. \tag{3.11}$$

The most straightforward way to use the Spectral–ROM from Eq. (3.10) is to apply a numerical integration scheme, *e.g.* an adaptive Runge–Kutta method with moderate accuracy, since Eq. (3.10) is just a ROM. So, with an embedded error control and not so

stringent tolerances, it can be done very efficiently. The exponential matrix is defined as the limit:

$$\mathrm{e}^{t\mathcal{A}} \;=\; \lim_{n\to\infty}\left(\mathrm{Id} \;+\; \frac{1}{n}\,t\,\mathcal{A}\right)^{n}.$$

in which $\mathrm{Id} \;\in\; \mathrm{Mat}_{(n-2)\times(n-2)}(\mathbb{R})$ is the identity matrix. However, this method is not the best way to compute the exponential matrix. In some particular cases, the solution of Eq. (3.10) can be simplified and thus better exploited [28].

Case I: If we have homogeneous boundary conditions, problem (3.10) becomes:

$$\begin{cases} \dot{a} &= \mathcal{A}\,(\nu)\,a\,, \\ a\,(t_0) &= a_0\,, \end{cases}$$

and it can be analytically solved as:

$$a\,(t\,;\nu) \;=\; \mathrm{e}^{(t\;-\;t_0)\,\mathcal{A}(\nu)}\cdot a_0\,.$$

Using modern methods, the exponential matrix can be computed using $\sim 48\,n^3$ *floating point operations per second* (FLOPS) [3]. As an information to the reader, the previous result was $\sim 538\,n^3$ FLOPS [21]. However, one can notice that we do not really need to build the exponential matrix, but we want to compute its *action* on the initial state vector a_0. Nowadays, it can be directly done, without forming $\mathrm{e}^{(t\;-\;t_0)\mathcal{A}(\nu)}$, explicitly to a prescribed accuracy that can be set significantly lower than the standard machine precision $\sim 10^{-16}$ [4]. If computing Eq. (3.10) by a `Matlab` solver, for example `ODE45`, the standard tolerance is of order of $\sim 10^{-6}$.

Case II: If we have inhomogeneous boundary conditions constant in time, the problem from Eq. (3.10) becomes:

$$\begin{cases} \dot{a} &= \mathcal{A}(\nu)\,a \;+\; \mathrm{b}\,(\nu)\,, \\ a(t_0) &= a_0\,, \end{cases}$$

which can also be analytically solved:

$$a\,(t\,;\nu) \;=\; \mathrm{e}^{(t\;-\;t_0)\,\mathcal{A}(\nu)}\,a_0 \;+\; (t-t_0)\,\frac{\mathrm{e}^{(t\;-\;t_0)\,\mathcal{A}(\nu)} \;-\; \mathrm{Id}}{(t\;-\;t_0)\,\mathcal{A}(\nu)}\,\mathrm{b}\,(\nu)\,.$$

Case III: If we have inhomogeneous boundary conditions are linear in time, problem Eq. (3.10) becomes:

$$\begin{cases} \dot{a} &= \mathcal{A}(\nu)\,a \;+\; \mathrm{b}\,(\nu)\cdot t\,, \\ a(t_0) &= a_0\,, \end{cases}$$

the solution is given by:

$$a\,(t\,;\nu) \;=\; \mathrm{e}^{(t\;-\;t_0)\,\mathcal{A}(\nu)}\,a_0 \;+\; (t\;-\;t_0)^2\,\frac{\mathrm{e}^{(t\;-\;t_0)\,\mathcal{A}(\nu)} \;-\; \mathrm{Id}}{(t\;-\;t_0)\,\mathcal{A}(\nu)}\,\mathrm{b}\,(\nu)\,.$$

Case IV: Boundary condition is polynomial in time:

$$\left\{ \begin{array}{rcl} \dot{a} & = & \mathcal{A}(\nu)\, a \;+\; \mathrm{b}\,(\nu) \cdot t^{\,m-1}\,, \quad m \;\geqslant\; 3\,, \\ a(t_0) & = & a_0\,. \end{array} \right.$$

then, the solution is given by the following analytical formula:

$$a\,(t\,;\nu) \;=\; \mathrm{e}^{\,(t\;-\;t_0)\,\mathcal{A}(\nu)}\, a_0 \;+\; (\,t \;-\; t_0\,)^{\,m}\; \varphi_m\Big(\,(\,t \;-\; t_0\,)\,\mathcal{A}(\nu)\Big)\,\mathrm{b}\,(\nu)\,.$$

Above we introduced the so–called matrix $\varphi-$functions:

$$\varphi_m(\,z\,) \;=\; \frac{\varphi_m(z) \;-\; \dfrac{1}{m!}}{z}\,, \qquad\qquad m \;\geqslant\; 0 \quad \text{with} \quad \varphi_0(\,z\,) \;\equiv\; \mathrm{e}^{\,z}\,.$$

A few first functions are given below explicitly:

$$\begin{aligned} \varphi_0(\,z\,) \;&=\; \mathrm{e}^{\,z} \;=\; 1 \;+\; z \;+\; \frac{1}{2}\,z^{\,2} \;+\; \frac{1}{3!}\,z^{\,3} \;+\; \ldots \\ \varphi_1(\,z\,) \;&=\; \frac{\mathrm{e}^{\,z}-1}{z} \;=\; 1 \;+\; \frac{1}{2}\,z \;+\; \frac{1}{3!}\,z^{\,2} \;+\; \frac{1}{4!}\,z^{\,3} \;+\; \ldots \\ \varphi_2(\,z\,) \;&=\; \frac{\mathrm{e}^{\,z}-1-z}{z^{\,2}} \;=\; \frac{1}{2} \;+\; \frac{1}{3!}\,z \;+\; \frac{1}{4!}\,z^{\,2} \;+\; \frac{1}{5!}\,z^{\,3} \;+\; \ldots \\ \varphi_3(\,z\,) \;&=\; \frac{\mathrm{e}^{\,z}-1-z-\frac{1}{2}}{z^{\,3}} \;=\; \frac{1}{3!} \;+\; \frac{1}{4!}\,z \;+\; \frac{1}{5!}\,z^{\,2} \;+\; \frac{1}{6!}\,z^{\,3} \;+\; \ldots \end{aligned}$$

The general power series representation of $\varphi-$functions is

$$\varphi_m(\,z\,) \;\equiv\; \sum_{k\,=\,0}^{\infty} \frac{z^{\,k}}{(m \;+\; k)!}\,.$$

The exponential definitions of $\varphi_m(\,z\,)$ should not be used for practical simulations, because of severe cancellation errors for $z \ll 1$. Efficient methods for computation of $\varphi-$functions have been developed based on PADÉ–type expansions, to give an example, `Matlab`'s function expm() is based on such approximations [10].

Case V: For a general case of linear boundary conditions, the solution of problem Eq. (3.10) is:

$$a\,(t\,;\nu) \;=\; \mathrm{e}^{\,(t\;-\;t_0)\,\mathcal{A}(\nu)} a_0 \;+\; \underbrace{\int_{t_0}^{\,t} \mathrm{e}^{\,(t\;-\;\tau)\,\mathcal{A}(\nu)}\,\mathrm{b}\,(\tau\,;\nu)\,\mathrm{d}\tau}_{(I)}\,.$$

To exploit the last formula, one might employ a quadrature formula to discretize the integral (I):

$$a\,(t\,;\nu) \;=\; \mathrm{e}^{\,(t\;-\;t_0)\,\mathcal{A}(\nu)} a_0 \;+\; \Delta t \sum_{j\,=\,1}^{m} \mathrm{e}^{\,(t\;-\;t_0)\,\mathcal{A}(\nu)} \cdot \mathrm{b}\,(\tau_j\,;\nu)\,, \qquad \Delta t :=\; \frac{t \;-\; t_0}{m}\,,$$

where we employed rectangle formula for simplicity. We note that the sequence $\{\mathrm{e}^{\,\Delta t\,\mathcal{A}(\nu)}\}_{j\,=\,1}^{m}$ can be entirely computed in an efficient manner [4].

Case VI: Considering a general nonlinear case of boundary conditions from problem Eq. (3.10) and the general solution Eq. (3.11). To exploit a better solution, we can develop the function $\tau \mapsto \mathrm{b}\,(\tau\,, a(\tau)\,;\nu)$ in TAYLOR expansion series and integrate it exactly:

$$a\,(t\,;\nu) \;=\; \mathrm{e}^{(t\,-\,t_0)\,\mathcal{A}(\nu)} a_0 \;+\; \sum_{k\,=\,1}^{\infty} (t\;-\;t_0)^{\,k}\,\varphi_k\Big((t\;-\;t_0)\,\mathcal{A}(\nu)\Big)\,a_k\,,$$

where

$$a_k \stackrel{\text{def}}{:=} \frac{\mathrm{d}^{\,k\,-\,1}}{\mathrm{d}t^{\,k\,-\,1}}\,\mathrm{b}\left(t\,, a(t)\,;\nu\right)\Big|_{\,t\;=\;t_0}\,.$$

Finally, the series solution can be exploited by truncating it at some finite order:

$$a\,(t\,;\nu) \;=\; \mathrm{e}^{(t\,-\,t_0)\,\mathcal{A}(\nu)} a_0 \;+\; \sum_{k\,=\,1}^{K} (t\;-\;t_0)^{\,k}\,\varphi_k\Big((t\;-\;t_0)\,\mathcal{A}\,(\nu)\Big)\,a_k\,.$$

In this study, we shall employ ODE solvers for simplicity, since we are interested in the whole trajectory.

3.2. Validation of the numerical solution

To compare and validate the proposed method, the error between a solution u, obtained by Spectral reduced order method or classical numerical methods, and the reference solution $u^{\,\mathrm{ref}}$, is computed as a function of x by the following formulation:

$$\varepsilon_{\,2}\,(x) \;\stackrel{\text{def}}{:=}\; \sqrt{\frac{1}{N_t}\sum_{j=1}^{N_t}\,\left(\,u_j^{\,\mathrm{num}}\,(x\,,t)\;-\;u_j^{\,\mathrm{ref}}\,(x\,,t)\,\right)^2}\,,$$

where N_t is the number of temporal steps. The global error $\varepsilon_{\,\infty}$ is given by the maximum value of $\varepsilon_{\,2}(x)$:

$$\varepsilon_{\,\infty} \;\stackrel{\text{def}}{:=}\; \sup_{\,x\;\in\;\left[\,0\,,\,L\,\right]}\;\varepsilon_{\,2}\,(x)\,.$$

The computation of the reference solution $u^{\,\mathrm{ref}}\,(x\,,t)$ is detailed in Sections 4.1, 4.2 and 5.1.

4. Numerical application

4.1. Linear case

A first case of linear moisture transfer is considered. From a physical point of view, the numerical values correspond to a material length of 0.1 m. The moisture transport coefficient is $d_{\,m} \;=\; 1.97{\cdot}10^{-10}\,\mathsf{s}$ and the moisture storage is $c_{\,m} \;=\; 7.09{\cdot}10^{-3}\,\mathsf{kg/m^3/Pa}$ [16]. The initial vapour pressure across the material is considered to be uniform as $P_v^{\,i} \;=\; 1.16{\cdot}10^3$

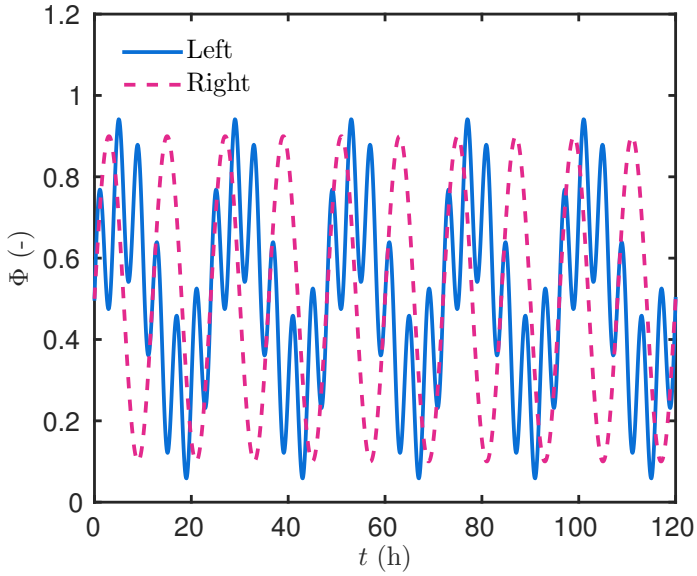

Figure 1. *Boundary conditions at the left side* ($x = 0\,\mathsf{m}$) *and at the right side* ($x = 0.1\,\mathsf{m}$).

Pa, corresponding to a relative humidity of 50%. Simulations are performed for a total time of 120h. The boundary conditions, represented by the relative humidity ϕ are given in Figure 1. The sinusoidal variations oscillate between dry and moist states during the total simulation time. The convective vapour transfer coefficients are set to $h_{v,\mathrm{L}} = 2\cdot10^{-7}$ s/m and $h_{v,\mathrm{R}} = 3\cdot10^{-8}$ s/m for the left and right boundaries, respectively. As the readers may be interested in simulate the proposed case, dimensionless values are provided in Appendix A.

The described case study is performed with the Spectral–ROM using $N = 6$ modes and with two central finite–difference approximations schemes: *(i)* the Euler implicit and *(ii)* the Crank–Nicolson. The reference solution is computed using the `Matlab` open source toolbox `Chebfun` [13].

The reduced system of ODEs is implemented in `Matlab` and the Spectral coefficients $\{a_n(t)\}$ are calculated for any intermediate time instant by the solver `ODE45`. The solver is set with an absolute and relative tolerance of $\mathsf{tol} = 10^{-4}$. In this work, all integrations in the time domain use an uniform discretization, although an adaptive approach can be used to improve even more the usage of the Spectral method. Computations of the Spectral solution are performed for the reference domain of $[-1, 1]$ and then transformed to the interested one.

It can be seen that the physical phenomena is well represented, as illustrated in Figure 2(a) with the evolution of the vapour pressure at $x = 0.04\,\mathsf{m}$. The variations follow the ones of the left boundary conditions and with the diffusion process going towards the periodic regime. It can be noted a good agreement between the Spectral–ROM and the other methods. Furthermore, the vapour pressure profile is shown in Figure 2(b) for

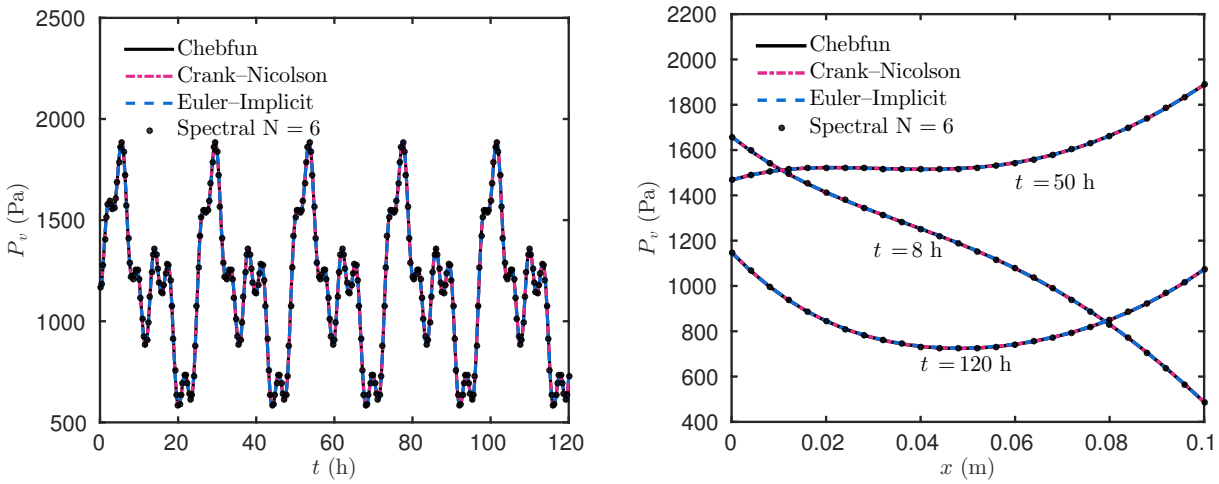

(a) (b)

Figure 2. *Evolution of the vapour pressure inside of the material, in* $x = 0.04$ m *(a) and vapour pressure profiles at different times, for* $t \in \{8, 50, 120\}$ h *(b).*

$t = \{8, 50, 120\}$ h, enhancing the good accuracy of the solution to represent the physical phenomena.

The absolute error ε_2 among the different methods and the reference is of the order of $\mathcal{O}(10^{-4})$, as illustrated in Figure 3. The solutions of the problem have been computed for discretisation parameters $\Delta x^\star = 4 \cdot 10^{-2}$ and $\Delta t^\star = 10^{-1}$ for both Spectral–ROM and for the Crank–Nicolson methods, while for the Euler implicit scheme more refinement was needed ($\Delta x^\star = 1 \cdot 10^{-2}$ and $\Delta t^\star = 10^{-2}$) to reach the same order of accuracy.

Figure 4(b) presents the absolute error ε_2 for the Spectral–ROM using different number of modes. As we increase the number of modes, the solution of the Spectral–ROM gets more accurate and the method solution converges within a few modes (less than 10). To illustrate the convergence of the solution, the profile of the vapour pressure for the last time of simulation is represented as a function of the number of modes in Figure 4(a). In this case, if we compare the solution with 3 modes to the solution with 5 modes a significant difference can be noticed. With 5 modes we already have a satisfactory solution of the problem, with the absolute error of order of $\mathcal{O}(10^{-3})$, while the solution with 3 modes is still oscillating. The number of modes of the Spectral method is predetermined in order to build the ODE system. In this case, a number of six modes proved to be good enough.

Spectral coefficients $a_n(t)$ are shown in Figures 5(a) and 5(b). It can be seen that the first coefficients have the most significant values. For this reason, the Spectral method needs few modes to converge to the solution (an order of 10) because its first modes have the highest magnitudes. A brief comparison with an analytical solution, built on Fourier decomposition [18], reveals that the eigenvalues of the Spectral method decreases faster, as shown in Figure 6. Note that the eigenvalues of the analytical solution do not have to coincide with the ones of the Spectral method since the eigenfunctions are not the same for the Chebyshev polynomials and the trigonometric ones.

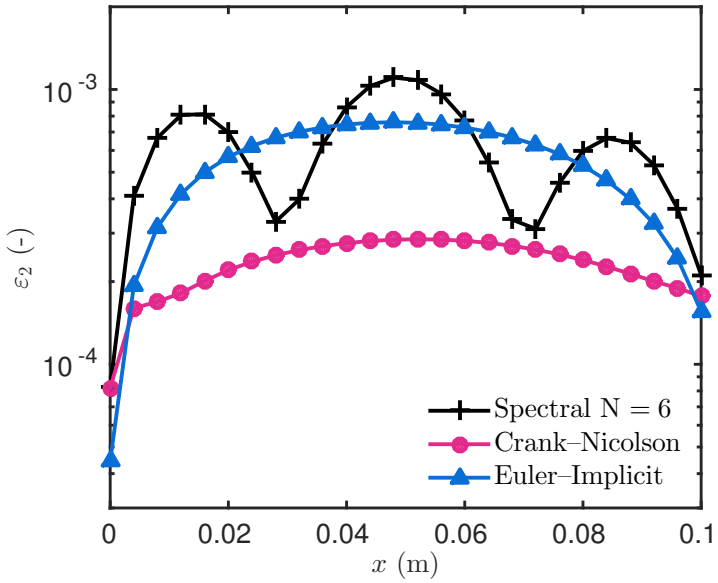

Figure 3. *Error ε_2 computed for the* Crank–Nicolson *method, for the* Euler *implicit and for the Spectral with $N = 6$ modes.*

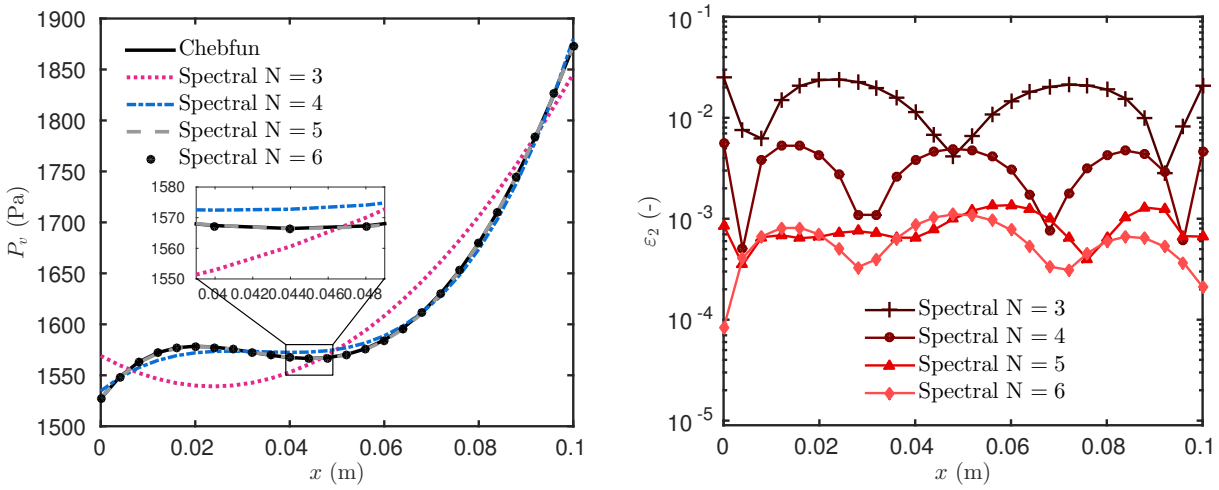

Figure 4. *Vapour pressure profiles (at $t = 2$ h) (a) computed with different numbers of Spectral modes and the error ε_2 (b).*

The global absolute error ε_∞ for all conventional numerical methods applied is calculated as a function of spatial discretisation $\Delta x^\star$. Fig. 7 shows that the Spectral–ROM has the same accuracy for all values of $\Delta x^\star$. It is due to the fact that the Spectral–ROM is based on Chebyshev polynomials, which enables to calculate the solution in each spatial node (the so–called collocation points in the Spectral approach), as the analytical solution. For this reason, the error of the Spectral solution is almost a straight line, not depending

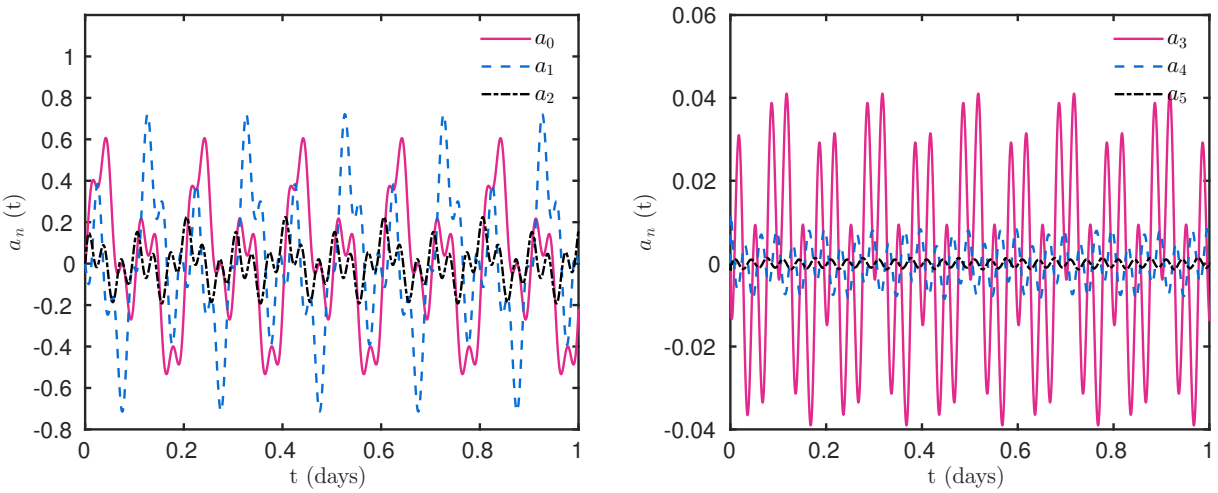

Figure 5. *Evolution of the first three Spectral coefficients a_n (a) and of the last three coefficients (b).*

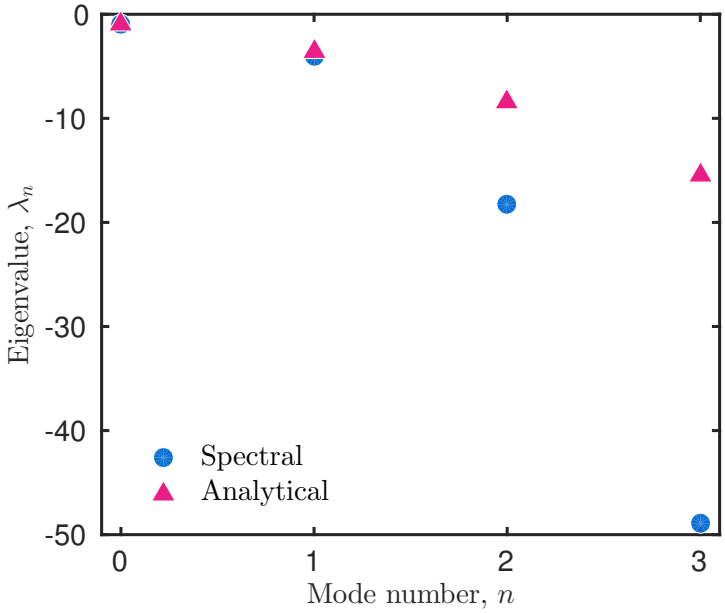

Figure 6. *Eigenvalues of the Analytical and of the Spectral solution corresponding to the first modes.*

on the spatial discretisation. However, for the conventional methods, the solution gets inaccurate when the value of $\Delta x^\star$ increases. It should be noted that the Spectral–ROM can provide even more accurate results, by increasing the number of modes or by decreasing the tolerance in the ODE `Matlab` solver to certain limits.

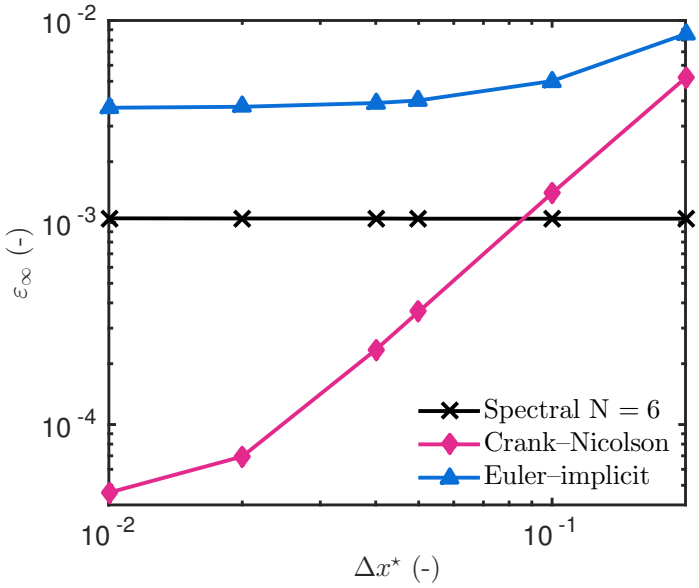

Figure 7. *Error ε_∞ in function of the $\Delta x^\star$ values.*

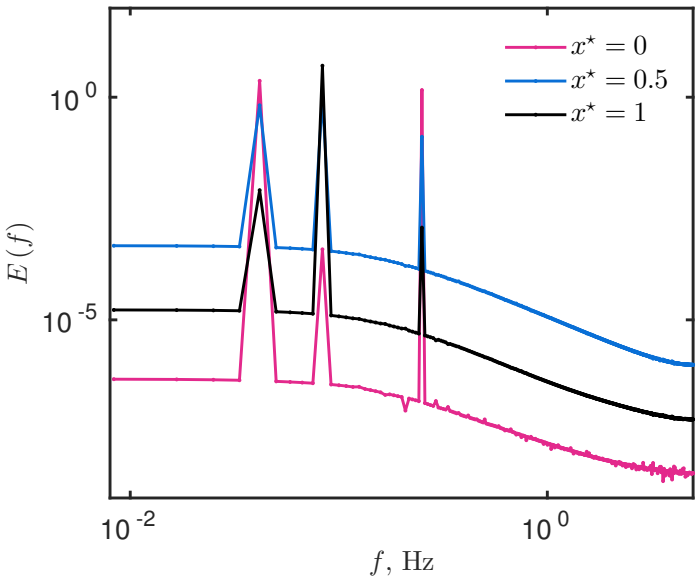

Figure 8. FOURIER power spectrum computed in the boundaries and in the middle of the material $x^\star \in \{0, 0.5, 1\}$.

Figure 8 shows the FOURIER power spectrum function of the signal frequency per unit of time, generated by the fast FOURIER transform. In this Figure, three peaks are observed in the signal frequency, coming from the boundary conditions. They occur because the relative humidity varies according to sinus functions.

4.2. Weakly nonlinear case

This case is called weakly nonlinear because the boundary conditions remain linear and, only the diffusion coefficient has a slight dependency on the moisture field. Thus, the diffusion equation is written as:

$$\frac{\partial u}{\partial t} \;=\; \nu(u)\,\frac{\partial^2 u}{\partial x^2}\,, \tag{4.1}$$

where, $\nu\,(u) \;=\; \nu_0 \;+\; \nu_1 \cdot u$. Since we have the diffusion coefficient depending on the field $\nu\,(u)$, the residual is written as:

$$R \;=\; \sum_{i=0}^{n} \left[\, \dot{a}_i(t) \;-\; \nu_0 \cdot \tilde{\tilde{a}}_i(t) \,\right] T_i(x) \;-\; \nu_1 \cdot \sum_{i=0}^{n} a_i(t)\, T_i(x) \cdot \sum_{k=0}^{n} \tilde{\tilde{a}}_k(t)\, T_k(x)\,.$$

Then, the residual is assumed orthogonal to the basis functions $\{T_i(x)\}$, leading to the following equation:

$$\dot{a}_i(t) \;=\; \nu_0 \cdot \tilde{\tilde{a}}_i(t) \;+\; \nu_1 \cdot \sum_{j=0}^{n} \sum_{k=0}^{n} c_{i,j,k}\, a_j(t)\, \tilde{\tilde{a}}_k(t)\,, \tag{4.2}$$

where,

$$c_{i,j,k} \;=\; \frac{2}{\pi} \int_{-1}^{1} \frac{T_i(x)\, T_j(x)\, T_k(x)}{\sqrt{1 \;-\; x^2}}\, \mathrm{d}x\,.$$

Equation (4.2) is a closed system of ODE that is expanded by using the Maple® software. Coefficients $c_{i,j,k}$ are calculated at once, and coefficient $\tilde{\tilde{a}}_i$ are related to a_i though a linear transformation $\tilde{\tilde{a}} \;=\; \mathrm{D}_2 \cdot a$, in which $\mathrm{D}_2 \in \mathrm{Mat}_{(n-2)\times(n-2)}(\mathbb{R})$ is a second order derivative matrix.

4.2.1 Case study

This case considers that c_m has a slight dependency on the moisture. The material piece has a length of 0.1 m , with a relative humidity-dependent diffusion coefficient:

$$\nu \;=\; \frac{d_m}{c_m} \;=\; 3.05 \cdot 10^{-8} + 6.94 \cdot 10^{-8} \cdot \phi\,.$$

The initial vapour pressure in the material is considered uniform $P_v^i \;=\; 1.16 \cdot 10^3$ Pa , corresponding to a relative humidity of 50% and to temperature of 20°C. Simulations are performed for a total time of 72 h, the equivalent of three days. The boundary conditions, represented by the relative humidity ϕ are given in Figure 9. The relative humidity oscillates sinusoidally between 50% and 75% on the left boundary and between 50% and 80% on the right boundary. The convective vapour coefficients are set to $h_{v,\mathrm{L}} \;=\; 3 \cdot 10^{-8}$ s/m and $h_{v,\mathrm{R}} \;=\; 2 \cdot 10^{-7}$ s/m for the left and right boundaries, respectively. The dimensionless values of this case are also provided in Appendix A.

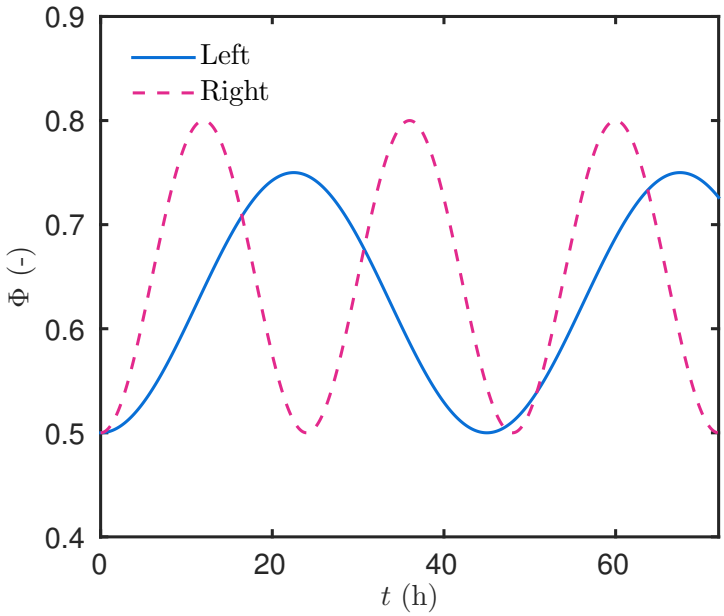

Figure 9. *Boundary conditions at the left side* ($x = 0\,\mathsf{m}$) *and at the right side* ($x = 0.1\,\mathsf{m}$) *of the domain.*

The Spectral reduced order model is composed by $N = 6$ modes and its coefficients $\{a_n(t)\}$ are obtained through the use of the solver `ODE45`, with a tolerance set to $\mathsf{tol} = 10^{-4}$. The discretisations used to compute the Spectral solution are $\Delta x^\star = 10^{-2}$ and $\Delta t^\star = 10^{-1}$.

The evolution of the vapour pressure in the middle of the material, at $x = 0.05\ \mathsf{m}$, is shown in Figure 10(a). The vapour pressure varies according to the sinusoidal fluctuations from both boundary conditions. The vapour pressure profiles at different times are illustrated in Figure 10(b) for $t = \{9, 38, 72\}\,\mathsf{h}$, highlighting the good agreement of the Spectral solution in representing the variations.

The absolute error ε_2 has been computed between the reference solution and the Spectral–ROM for different number of modes, as illustrated in Figure 11. For $N = 6$ and $N = 5$ modes the absolute error is at the same order, $\mathcal{O}(10^{-3})$, proving the accuracy of the solution and showing 5 modes are good enough.

Figures 12(a) and 12(b) present the first three and the last coefficients a_n, respectively. The magnitude of the coefficient, in the total contribution of the solution, decreases with the order of the coefficient. The last coefficient determines the magnitude of the error, implying that the error will never be lower than the magnitude of the last coefficient a_n. It is due to the truncation in the number of terms in the separated representation of the solution. Thus, the higher the number of modes, the higher the accuracy. For this case, we can not have a more precise solution than $\sup_{t \in [0,T]} |a_6| = 1.3 \cdot 10^{-3}$. This happens because of the truncation error in the number of terms.

Figure 13 indicates the Fourier power spectrum as a function of the signal frequency, generated by the fast Fourier transform. For the left boundary, only one peak of the

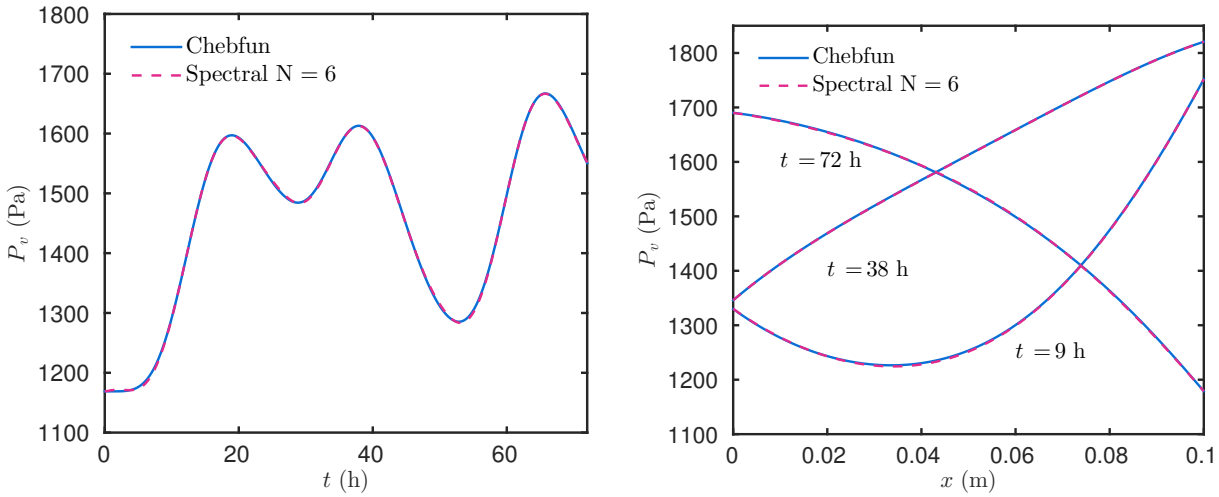

Figure 10. *Evolution of the vapour pressure inside of the material, in* $x = 0.05$ m *(a) and vapour pressure profiles at different times, for* $t \in \{9, 38, 72\}$ h *(b).*

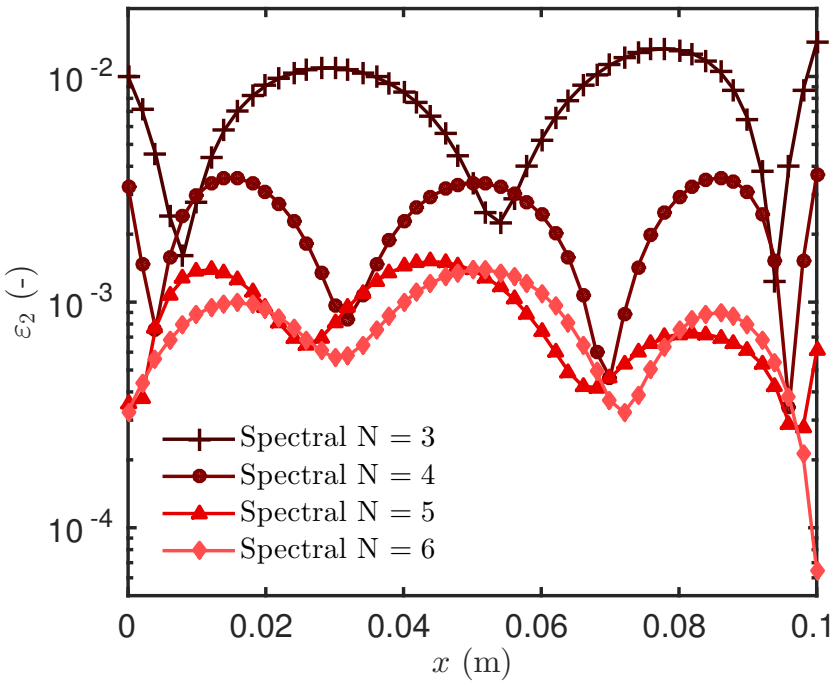

Figure 11. *Error* ε_2 *computed for the Spectral solution, varying the number of modes.*

signal can be observed, indicating that there is no flux arriving from the other boundary. The peaks in the middle of the material corresponds to the information arriving from both boundaries. On the right side, more peaks appear than the two signals coming from the boundaries, due to the low nonlinearity present in the diffusion process.

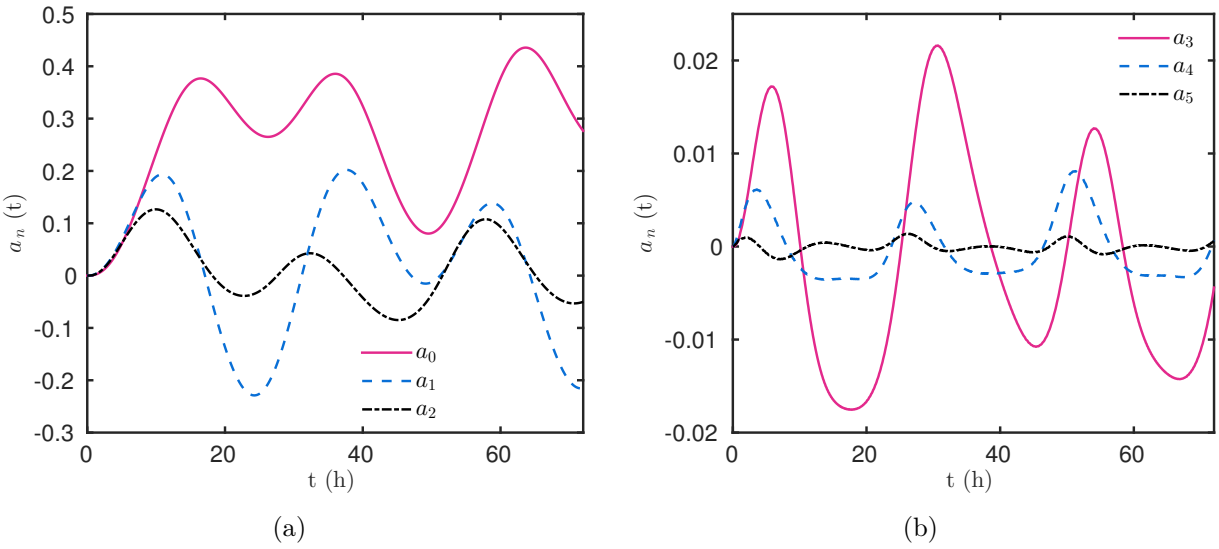

Figure 12. *Evolution of the first three Spectral coefficients a_n (a) and of the last three coefficients (b).*

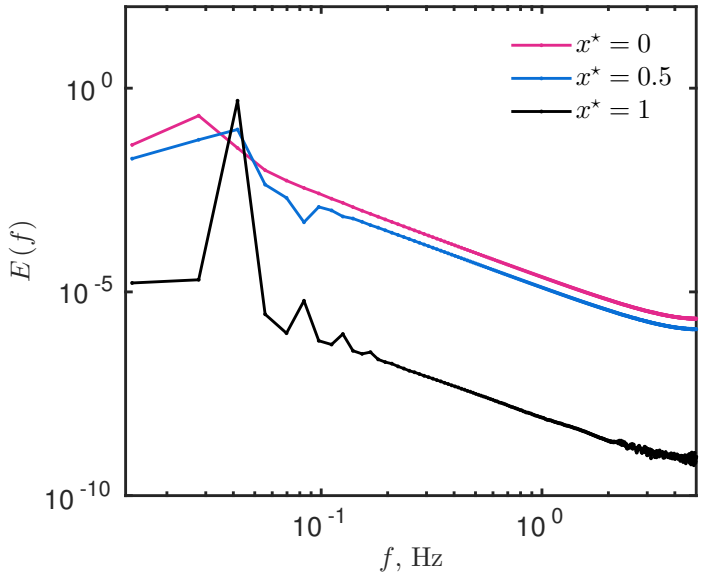

Figure 13. FOURIER *power spectrum computed in the boundaries and in the middle of the material* $x^\star \in \{0, 0.5, 1\}$.

4.3. Numerical cost

4.3.1 Linear case

The number of operations for each approach can be estimated. We denote for N_x and N_t the number of nodes according to the discretisation in both space and time domains. For explicit methods, it can be related by CFL type conditions. A standard approach based on the Euler implicit scheme requires $N_x \cdot N_t$, operations while the Crank–Nicolson scheme requires at least twice as many, as it is built on both implicit and explicit parts. Considering the discretisation parameters $N_t = 1200$ and $N_x = 100$, the number of operations scales with:

$$\begin{aligned} &\text{Euler implicit:} && \mathcal{O}\Big(N_x \cdot N_t \Big) \simeq \mathcal{O}\Big(1.2 \cdot 10^5 \Big), \\ &\text{Crank–Nicolson:} && \mathcal{O}\Big(2 \cdot N_x \cdot N_t \Big) \simeq \mathcal{O}\Big(2.4 \cdot 10^5 \Big). \end{aligned}$$

For the Spectral–ROM, the number is related to the solution of the ODE system Eq. (3.8), computed in this case with the `Matlab` solver `ODE45`. It is based on the iterative Runge–Kutta method to approximate the solution. The number of operation depends on the tolerance (tol) of the solver, which has a maximum tolerance of $\sim 10^{-5}$ for `ODE45`. Thus, we have:

$$N_t \simeq \frac{T}{\Delta T} \simeq \frac{T}{(\mathsf{tol})^{1/5}},$$

where T is the total time of simulation. At each time step, the Runge–Kutta needs to compute six times the right-hand side. For linear systems it is $\mathcal{A} \times a\,(t_s)$, where s depends on the degree of freedom N of the solution ($s = N - 2$). Thus, it leads to $6 \cdot s^2$ operations to perform, knowing that s is of order of 10. Consequently, the total number of operations for the Spectral–ROM scales with approximately:

$$\mathcal{O}\left(\frac{6\,(N-2)^2\,T}{(\mathsf{tol})^{1/5}} \right).$$

Considering the first case, knowing that the tolerance was set to 10^{-4}, with $N = 6$ modes the number of operations performed by the Spectral–ROM is expressed by:

$$\text{Spectral–ROM:} \quad \mathcal{O}\left(\frac{6\,(N-2)^2\,T}{(10^{-4})^{1/5}} \right) \simeq \mathcal{O}\Big(35 \cdot (6-2)^2 \cdot 120 \Big) \simeq \mathcal{O}\Big(6.7 \cdot 10^4 \Big).$$

Comparing the number of operations of this case, we can already see that the Spectral–ROM is less costly than the other methods applied. Notice that the number of degrees of freedom necessary to solve the diffusion problem by means of the Spectral method is inferior to the ones necessary to solve the whole system of partial differential equations. Using Euler or Crank–Nicolson methods, the order of the solution scales with $p = N_x$, whereas the one Spectral–ROM is $s = (N - 2)$. For this case, the numerical application gives $p \equiv 10^2$ and $s \equiv 4$. Moreover, we can note the reduction of the order of the solution, using the Spectral approach. According to the previous results, the fidelity of the model is not degraded but only the order of the solution.

4.3.2 Weakly nonlinear case

The time spent on simulations is also related to the solver used to compute ODE system. For the weakly nonlinear case, different solvers were employed with two different values of tolerances. The values of the maximum absolute error and of the CPU time are reported in Table 1. Considering the Spectral method with $N = 6$ modes, even if we increase the precision of the solver, the error is limited by the magnitude of the last Spectral coefficient. All solvers provided almost the same value for the absolute maximum error. In addition, for the CPU time, the fastest solver was the `ODE15s`, but the difference from the other solvers was not significant. When we increase the number of modes to $N = 9$, more distinct the results are. As we have more modes, the last Spectral coefficient is even smaller, and thus, the solution can be more accurate. By decreasing the tolerance of the solver, it was possible to have more accurate results. Therefore, depending on the accuracy sought on the results, several options are available. Although, the solver `ODE15s` showed to be the most efficient, it combines also accuracy and rapidness.

The choice of the ODE solver is related to the problem nature. For example, if the problem has two components which vary drastically on different time scales, then the problem is stiff, or difficult in evaluation. The solvers are then classified according to the problem type. For non-stiff problems, `ODE45`, `ODE23` and `ODE113` are the most appropriate, but for stiff problems, the other ODE solvers are indicates. Further information can be found in [34].

5. Treating general nonlinearities

Problem (2.6) has an important difficulty in dealing with the nonlinearities of the moisture storage coefficient c_m and of the diffusion coefficient d_m, both depending on the moisture content field. These coefficients are usually given by empirical functions from experimental data. Due to those nonlinearities, some modifications in the way of using the Spectral method have to be taken into account. For this reason, Eq. (2.6a) is recalled with a simplified notation:

$$c_m(u)\frac{\partial u}{\partial t} = \frac{\partial}{\partial x}\left[d_m(u)\frac{\partial u}{\partial x}\right]. \tag{5.1}$$

In order to apply better the Spectral method, Eq. (5.1) is rearranged as follows:

$$\frac{\partial u}{\partial t} = \nu(u)\frac{\partial^2 u}{\partial x^2} + \lambda(u)\frac{\partial u}{\partial x}, \tag{5.2}$$

where,

$$\nu(u) \overset{\text{def}}{:=} \frac{d_m(u)}{c_m(u)},$$

$$\lambda(u) \overset{\text{def}}{:=} \frac{1}{c_m(u)} \cdot \frac{\mathrm{d}(d_m(u))}{\mathrm{d}u}.$$

Table 1. *CPU time and maximum absolute error ε_∞ computed with the different ODE solvers.*

$N = 6$	tol $= 10^{-4}$		tol $= 10^{-6}$	
Solver	ε_∞	CPU time (s)	ε_∞	CPU time (s)
`ODE45`	$1.38 \cdot 10^{-3}$	$6.50 \cdot 10^{-1}$	$1.38 \cdot 10^{-3}$	$3.97 \cdot 10^{-1}$
`ODE23`	$1.39 \cdot 10^{-3}$	$5.30 \cdot 10^{-1}$	$1.42 \cdot 10^{-3}$	$4.65 \cdot 10^{-1}$
`ODE113`	$1.39 \cdot 10^{-3}$	$3.69 \cdot 10^{-1}$	$1.38 \cdot 10^{-3}$	$4.43 \cdot 10^{-1}$
`ODE15s`	$1.39 \cdot 10^{-3}$	$2.31 \cdot 10^{-1}$	$1.43 \cdot 10^{-3}$	$1.93 \cdot 10^{-1}$
`ODE23s`	$1.39 \cdot 10^{-3}$	1.90	$1.42 \cdot 10^{-3}$	$6.39 \cdot 10^{-1}$
`ODE23t`	$1.39 \cdot 10^{-3}$	$3.90 \cdot 10^{-1}$	$1.39 \cdot 10^{-3}$	$2.91 \cdot 10^{-1}$
`ODE23tb`	$1.39 \cdot 10^{-3}$	$5.04 \cdot 10^{-1}$	$1.39 \cdot 10^{-3}$	$2.10 \cdot 10^{-1}$

$N = 9$	tol $= 10^{-4}$		tol $= 10^{-6}$	
Solver	ε_∞	CPU time (s)	ε_∞	CPU time (s)
`ODE45`	$1.45 \cdot 10^{-4}$	24.9	$3.50 \cdot 10^{-5}$	29.3
`ODE23`	$3.50 \cdot 10^{-4}$	16.3	$3.52 \cdot 10^{-5}$	23
`ODE113`	$1.05 \cdot 10^{-3}$	18.8	$3.55 \cdot 10^{-5}$	18
`ODE15s`	$1.28 \cdot 10^{-4}$	1	$3.52 \cdot 10^{-5}$	1
`ODE23s`	$1.03 \cdot 10^{-4}$	8.89	$3.52 \cdot 10^{-5}$	54.6
`ODE23t`	$1.42 \cdot 10^{-4}$	1.33	$3.48 \cdot 10^{-5}$	3.66
`ODE23tb`	$1.63 \cdot 10^{-4}$	1.8	$3.46 \cdot 10^{-5}$	7.17

By using Spectral methods the unknown $u(x, t)$ is approximated by the finite sum (3.3) and, the derivatives can be written in a way where the Chebyshev polynomials remain the same, as in the linear case of Eq. (3.4). Thus, Eq. (5.2) becomes:

$$\sum_{i=0}^{n} \dot{a}_i(t)\, T_i(x) \;=\; \nu\left(\sum_{i=0}^{n} a_i(t)\, T_i(x)\right) \sum_{i=0}^{n} \tilde{\tilde{a}}_i(t)\, T_i(x) + \lambda\left(\sum_{i=0}^{n} a_i(t)\, T_i(x)\right) \sum_{i=0}^{n} \tilde{a}_i(t)\, T_i(x)\,.$$

By applying the Galerkin projection we have:

$$\mathcal{M} \cdot \dot{a}_i(t) \;=\; \mathrm{G}_{i,j}\Big(\{a_i\}\Big) \cdot \tilde{\tilde{a}}_i(t) \;+\; \Lambda_{i,j}\Big(\{a_i\}\Big) \cdot \tilde{a}_i(t)\,, \tag{5.3}$$

where,

$$\mathrm{G}_{i,j}\Big(\{a_i\}\Big) \;=\; \int_{-1}^{1} \frac{\nu\,(\sum)\,T_i(x)\,T_j(x)}{\sqrt{1\;-\;x^2}}\,\mathrm{d}x\,,$$
$$\Lambda_{i,j}\Big(\{a_i\}\Big) \;=\; \int_{-1}^{1} \frac{\lambda\,(\sum)\,T_i(x)\,T_j(x)}{\sqrt{1\;-\;x^2}}\,\mathrm{d}x\,.$$

Using the Chebyshev–Gauss quadrature, the integrals are also approximated by a finite sum:

$$\mathrm{G}_{i,j}\Big(\{a_i\}\Big) \;\approx\; \frac{\pi}{m}\sum_{k=1}^{m} \nu_k\,T_i(x_k)\,T_j(x_k)\,,$$
$$\Lambda_{i,j}\Big(\{a_i\}\Big) \;\approx\; \frac{\pi}{m}\sum_{k=1}^{m} \lambda_k\,T_i(x_k)\,T_j(x_k)\,,$$

where,

$$\nu_k \;\overset{\text{def}}{:=}\; \nu\left(\sum_{i=0}^{n} a_i(t)\,T_i(x_k)\right),$$
$$\lambda_k \;\overset{\text{def}}{:=}\; \nu\left(\sum_{i=0}^{n} a_i(t)\,T_i(x_k)\right),$$

and x_k are the Chebyshev nodes:

$$x_k \;=\; \cos\left(\frac{2\,k\;-\;1}{2\,m}\,\pi\right).$$

The value of m is determined according to numerical investigations and will be discussed for the next case study.

In addition, we have the expressions of the nonlinear boundary conditions:

$$d_m\left(\sum_{i=0}^{n}\tilde{a}_i(t)\,(-1)^i\right)\sum_{i=0}^{n}\tilde{a}_i(t)\,(-1)^i \;-\; \mathrm{Bi}_{v,\mathrm{L}}\sum_{i=0}^{n}a_i(t)\,(-1)^i \;+\; \mathrm{Bi}_{v,\mathrm{L}}\cdot u_{\mathrm{L}} \;=\; 0\,, \tag{5.4a}$$

$$-d_m\left(\sum_{i=0}^{n}\tilde{a}_i(t)\right)\sum_{i=0}^{n}\tilde{a}_i(t) \;-\; \mathrm{Bi}_{v,\mathrm{R}}\sum_{i=0}^{n}a_i(t) \;+\; \mathrm{Bi}_{v,\mathrm{R}}\cdot u_{\mathrm{R}} \;=\; 0\,. \tag{5.4b}$$

Contrarily to the linear case, the boundary conditions cannot provide an explicit expression for the two last coefficients $a_n(t)$ and $a_{n-1}(t)$. Thus, it is not possible to compute the solution in the same way. Although, with all elements listed before, it is possible to set the system to be solved by composing an ODE system with two additional algebraic expressions for the boundary conditions. It results in a system of Differential–Algebraic Equations (DAEs) with the following form:

$$\mathcal{M}\,\dot{a}_n(t) \;=\; \mathcal{A}\,a_n(t) \;+\; b(t)\,, \tag{5.5}$$

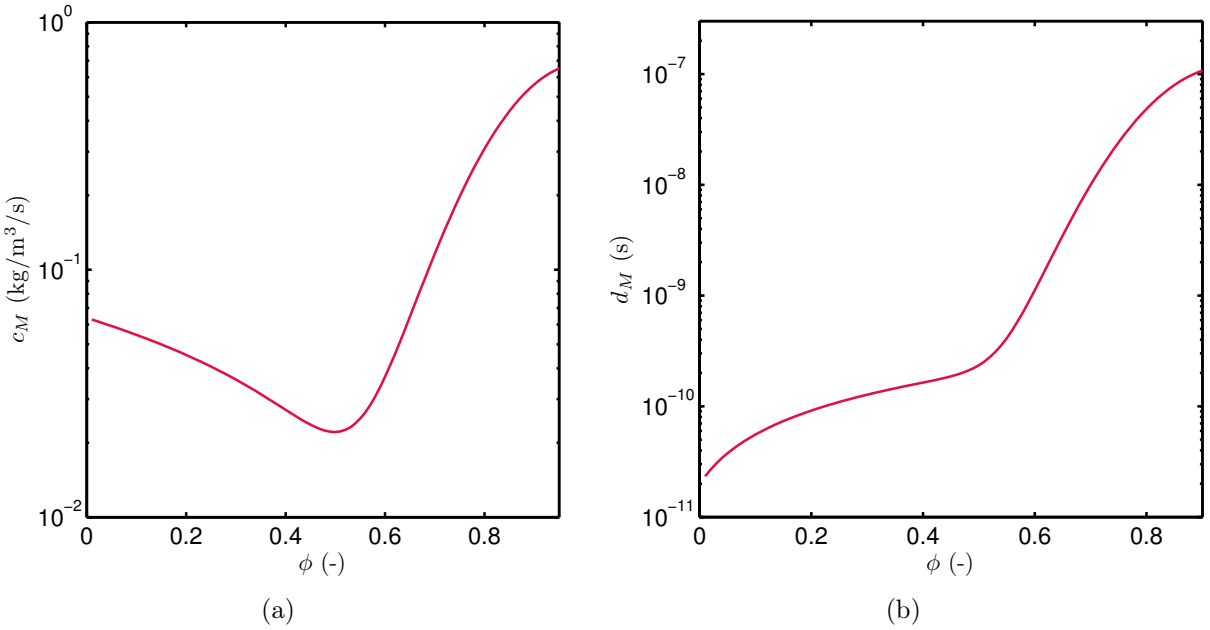

Figure 14. *Variation of the moisture storage c_m (a) and diffusion d_m (b) as a function of the relative humidity ϕ.*

where, $\mathcal{M}$ is a diagonal matrix containing the coefficients of the Chebyshev weighted orthogonal system, $b(t)$ is a vector containing the boundary conditions and, $\mathcal{A} \cdot a_n(t)$ is composed by the right member of equation (5.3). The initial condition is given by Eq. (3.9) and the DAE system is solved by `ODE15s` or `ODE23t` from `Matlab`.

5.1. A highly nonlinear case

This case study considers moisture dependent coefficients c_m and d_m, illustrated in Figures 14(a) and 14(b). Their variations are similar to the load bearing material from [19]. The initial vapour pressure is uniform $P_v^i = 1.16 \times 10^3$ Pa. No moisture flow is taken into account at the boundaries. The ambient vapour pressures at the boundaries are illustrated in Figure 15. At the left boundary, it has a fast drop until the saturation state and at the right boundary, it has a sinusoidal variation. The material is thus excited until the capillary state. The convective vapour transfer coefficients are set to $h_{v,\mathrm{L}} = 2 \cdot 10^{-7}$ s/m and $h_{v,\mathrm{R}} = 3 \cdot 10^{-8}$ s/m for the left and right boundary, respectively. The final simulation time is also fixed to 120 hours. As in the previous case study, the dimensionless values can be found in Appendix A.

The Spectral method is composed by $N = 9$ modes with $m = 7$. The `ODE15s` was used to solved the System (5.5), with a tolerance of 10^{-4}. For this case, the Spectral method was compared to the Crank–Nicolson [16] and to a reference solution computed using the `Chebfun Matlab` package [13]. All solutions have been computed with the following discretisation parameters: $\Delta t^\star = 10^{-1}$ and $\Delta x^\star = 10^{-2}$.

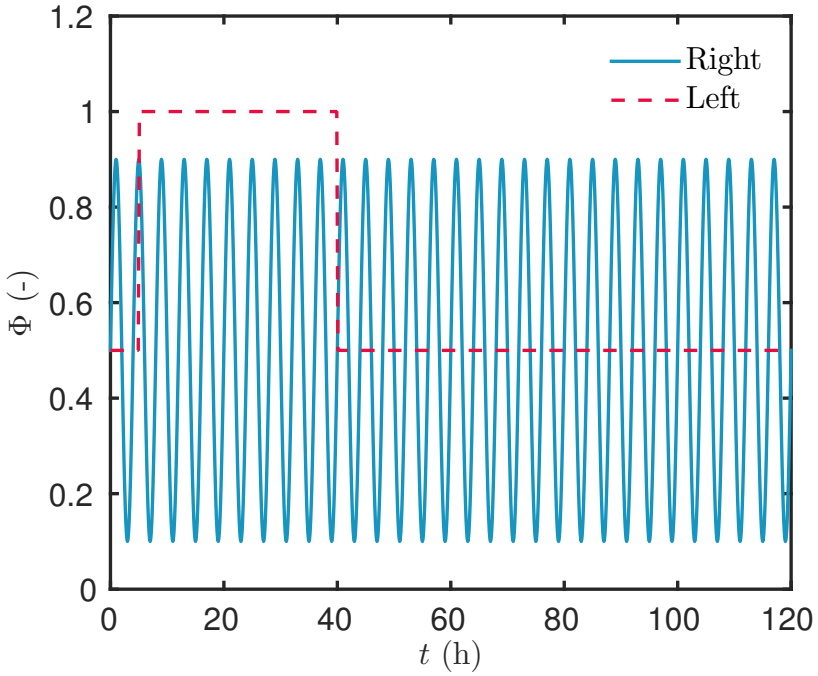

Figure 15. *Boundary conditions at the left side* ($x = 0$) *and at the right side* ($x = 0.1$).

Vapour pressure variations as boundary conditions are shown in Figure 16(a). The vapour pressure at $x = 0.1$ m slowly oscillates according to the right boundary condition. It also increases within the material according to the step imposed at the left boundary $x = 0$ m. This increasing can also be observed on three profiles of vapour pressure illustrated in Figure 16(b), in which the diffusion process is represented going from left to right.

All methods have demonstrated good agreement to represent the physical phenomenon. Again, the fidelity of the model does not deteriorate with the use of a Spectral approach. Results of the error ε_2 in function of x are shown in Figure 17(a). The error of the Crank–Nicolson scheme is proportional to $\mathcal{O}(\Delta t^{\star 2})$. The Spectral method with $N = 9$ modes is one order more accurate than the Crank–Nicolson method, even considering the same discretization parameters $\Delta t^\star$ and $\Delta x^\star$. Although, if we decrease the number of modes to $N = 6$ and maintaining the same discretization parameters $\Delta t^\star$ and $\Delta x^\star$, we reach the same order of accuracy of the Crank–Nicolson method, as observed in Figure 17(b).

The solution of the Spectral methods becomes more accurate with the increase of the the number of modes, as shown in Figure 17(b). With 6 modes, we have satisfactory results, with error of the order of $\mathcal{O}(10^{-3})$. As we increase only the number of modes, without changing other parameters, the error begins to stabilize, and with 8 and 9 modes the error remains the same.

As already observed in the linear case, the Spectral method does not depend on the number of spatial points, but on the order of the ODE solver tolerance and also on the

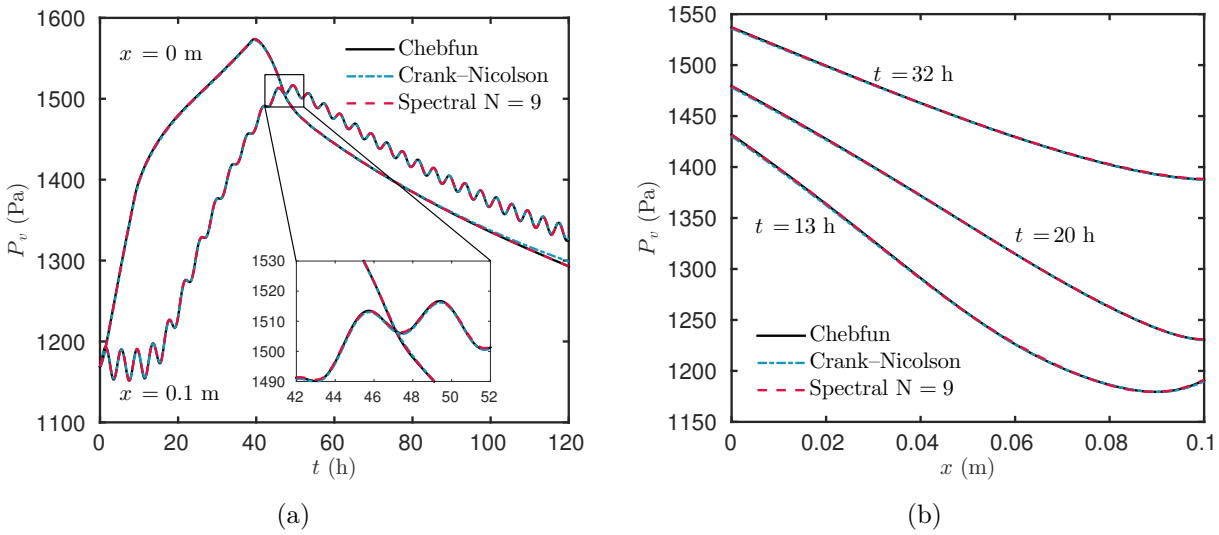

Figure 16. *Evolution of the vapour pressure at the boundaries,* $x \in \{0, 0.1\}$ m *(a) and vapour pressure profiles for* $t \in \{13, 20, 30\}$ h *(b).*

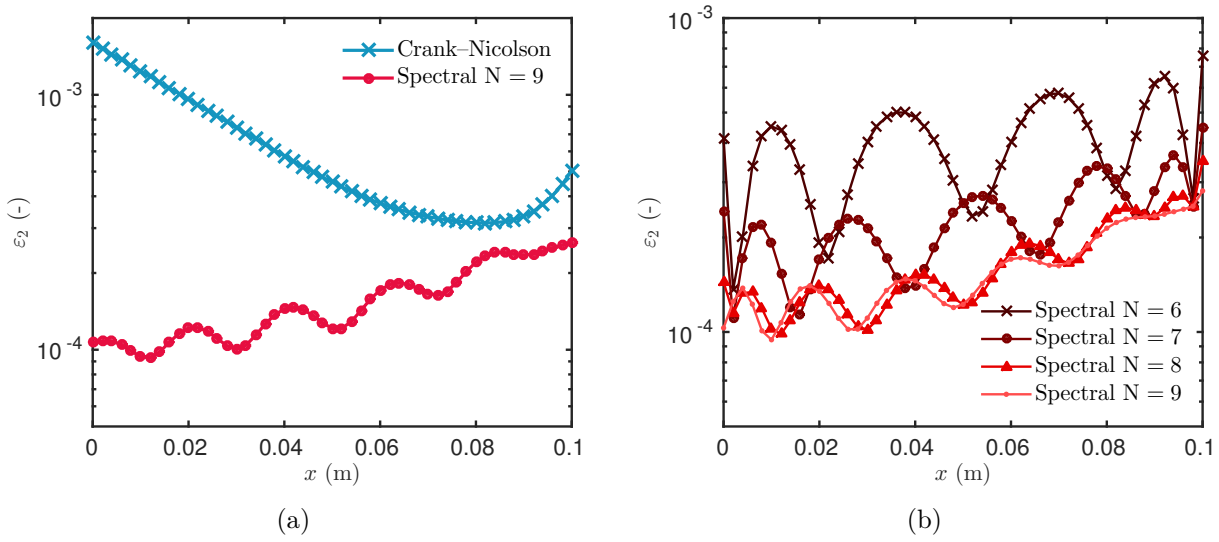

Figure 17. *Error* ε_2 *computed for the* Crank–Nicolson *method and for the Spectral with* $N = 9$ *modes (a), and the error* ε_2 *computed for the Spectral method with different number of modes (b).*

number of modes. For the nonlinear case, the error also depends on the truncation of the sum $\sum_{k=1}^{m}$. For this reason, the error ε_∞ in function of m is shown in Table 2. The optimal m number is approximated by numerical experimentation, and as can be seen in the Table, the best value for m is the one equivalent to the number of modes.

Figures 18(a) and 18(b) represent the first and last three coefficients a_n of the Spectral–ROM solution. The step in the left boundary can be also seen in these figures for the

Table 2. *Absolute error ε_∞ for different number of modes N and different truncations m.*

	$N = 5$	$N = 6$	$N = 7$	$N = 8$	$N = 9$
$m = 2$	$7.0 \cdot 10^{-2}$	—	$2.90 \cdot 10^{-1}$	—	—
$m = 3$	$2.8 \cdot 10^{-3}$	$2.02 \cdot 10^{-2}$	$1.94 \cdot 10^{-2}$	—	—
$m = 4$	$2.7 \cdot 10^{-3}$	$1.43 \cdot 10^{-3}$	$3.06 \cdot 10^{-3}$	$2.46 \cdot 10^{-2}$	$2.89 \cdot 10^{-1}$
$m = 5$	$2.6 \cdot 10^{-3}$	$1.54 \cdot 10^{-3}$	$9.30 \cdot 10^{-4}$	$1.05 \cdot 10^{-3}$	$4.13 \cdot 10^{-3}$
$m = 6$	$2.6 \cdot 10^{-3}$	$1.39 \cdot 10^{-3}$	$7.07 \cdot 10^{-4}$	$3.40 \cdot 10^{-4}$	$4.41 \cdot 10^{-4}$
$m = 7$	$2.6 \cdot 10^{-3}$	$1.40 \cdot 10^{-3}$	$6.59 \cdot 10^{-4}$	$3.20 \cdot 10^{-4}$	$2.60 \cdot 10^{-4}$
$m = 8$	$2.6 \cdot 10^{-3}$	$1.39 \cdot 10^{-3}$	$6.70 \cdot 10^{-4}$	$3.20 \cdot 10^{-4}$	$1.90 \cdot 10^{-4}$
$m = 9$	—	—	—	$3.09 \cdot 10^{-4}$	$2.40 \cdot 10^{-4}$
$m = 10$	—	—	—	$3.09 \cdot 10^{-4}$	$2.40 \cdot 10^{-4}$

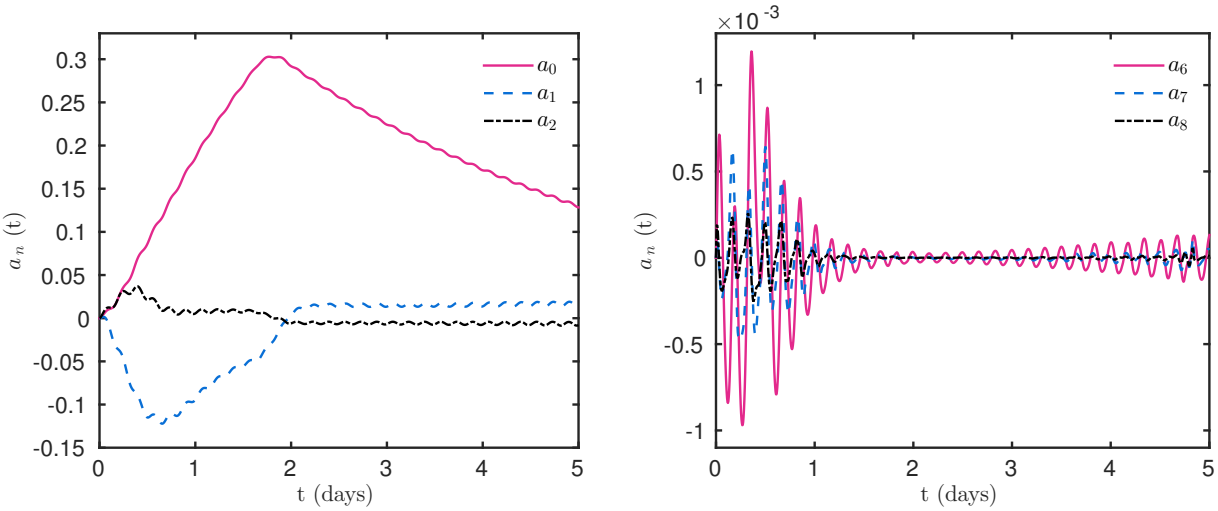

Figure 18. *Evolution of the first three (a) and of the last three (b) Spectral coefficients a_n.*

first days, and after that the values tend to stabilize. It is possible to see the reduction in the magnitude of the coefficient with the increase of the number of coefficients. As for the previous cases, the last coefficients are always the smallest ones. Figure 19 indicates the energy in function of the signal frequency per unit of time, obtained by performing a FOURIER transform. Only one peak in the signal frequency is observed, corresponding to the step in the relative humidity occurring at the left boundary.

A parametric study is performed in order to verify the computational cost of the proposed method. The discretisation parameters are set to $\Delta x^\star = 10^{-2}$ and $\Delta t^\star = 10^{-2}$,

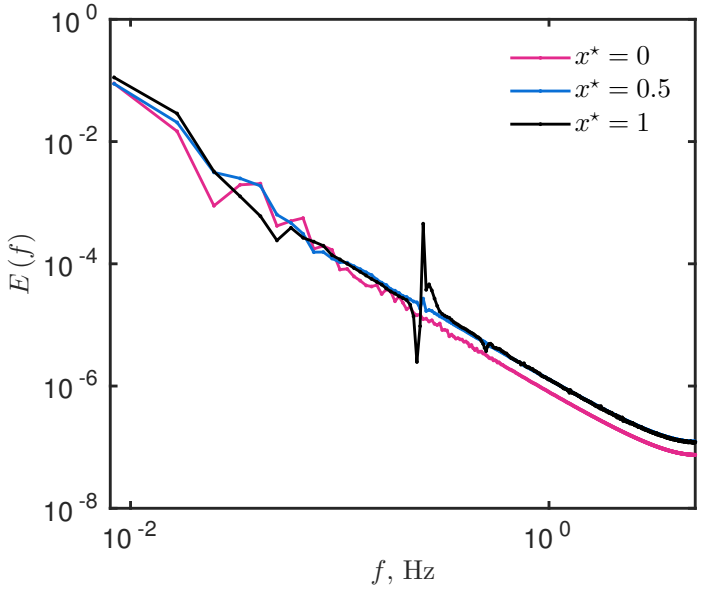

Figure 19. Fourier *power spectrum computed in the boundaries and in the middle of the material* $x^\star \in \{0, 0.5, 1\}$.

while the number of modes N of the Spectral solution and the tolerance of the solver vary. Figure 20(a) presents the maximum absolute error ε_∞ in function of the number of Spectral modes. As we increase the number of modes, the solution gets more accurate. Although, after a certain number of modes, the solution converges to a minimum value, that is related to the tolerance of the ODE solver. The time to perform each Spectral simulation is presented in Figure 20(b). For this numerical application, the CPU time has been evaluated using `Matlab` platform on a computer with Intel i7 CPU and 8GB of RAM. The computational effort to perform the simulation increases linearly with the number of modes. However, it remains extremely low. To better appreciate the computational cost of each approach, Table 3 provides the CPU time to compute the solution using the Crank–Nicolson scheme, the `Chebfun` package for the same discretisation parameters. The Spectral solution has been computed with $N = 9$ modes. It is preferable to focus on the ratio of computer run time rather than on absolute values, that are system-dependent. Even with an average number of sub-iterations is $\mathcal{O}(N_{\mathrm{NL}}) = 1$ of the Crank–Nicolson scheme, the Spectral method is substantial faster then the other methods. It represents only 1% of the CPU time needed using the Crank–Nicolson approach.

6. Conclusions

Most of the numerical methods applied to mathematical models used in building physics are commonly based on implicit schemes to compute the solution of diffusion problems. Its main advantage is due to the stability conditions for the choice of the time step $\Delta t^\star$.

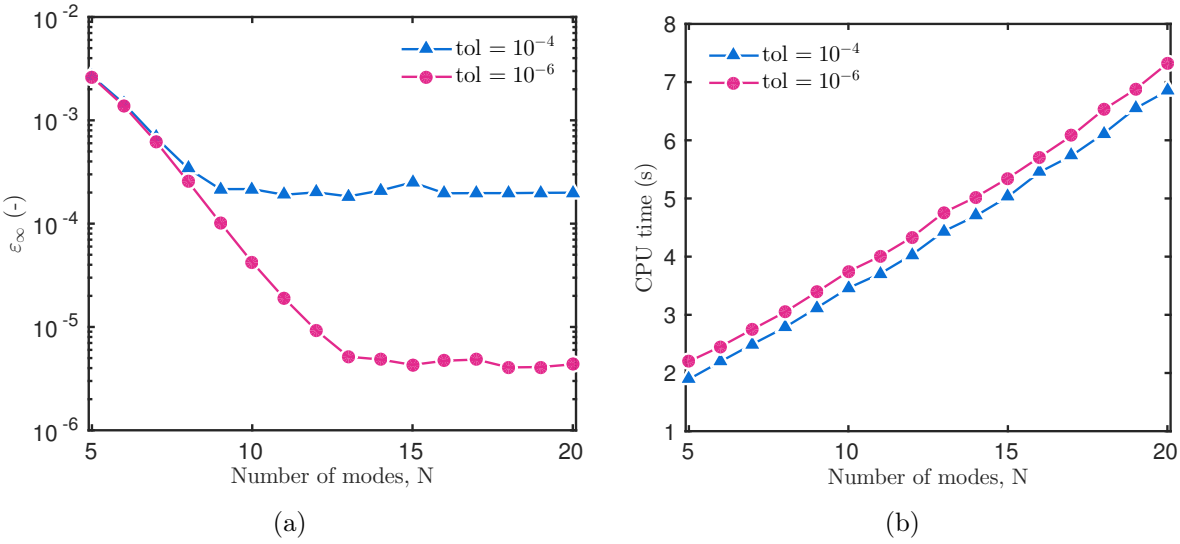

(a) (b)

Figure 20. *Maximum absolute error as a function of the number of Spectral modes (a) and their respective CPU simulation time (b).*

Table 3. *Computational time required for the numerical schemes perform the nonlinear case ($\Delta x^\star = 10^{-2}$ and $\Delta t^\star = 10^{-2}$).*

Numerical Scheme	CPU time (s)	CPU time (%)	Average number of iterations
Spectral $N = 9$	3	1	—
`Chebfun`	96	29	—
Crank–Nicolson	327	100	1

However, implicit schemes require important sub–iterations when treating nonlinear problems. This work was therefore devoted to explore the use of an innovative reduced order approach based on the Spectral method. Spectral methods are well-known in other applications, such as meteorology and wave propagation, although it was not used before as a reduction order model. Thus, in this work we showed that they can by applied in building physics problems to compute a reduced order model. Its application is not straight forward as it requires a pre-treatment of the problem, but the results are very promising. The first case study considered a linear diffusive moisture transfer through a porous material. The Spectral–ROM was compared to the classical Euler implicit scheme, to the Crank–Nicolson scheme and to a reference solution obtained using Chebyshev polynomials. Results have shown the dynamics and amplitude of hygrothermal fields are perfectly represented by the Spectral–ROM solution. The fidelity of the physical model is totally conserved by the Spectral–ROM. Only the order of the solution is highly reduced. Using standard approaches, the order of the solution rises with 10^2 whereas with the Spectral

method, the order of the solution scales with 4 . In the second case, a weak nonlinear problem was treated, which has a field dependent diffusion coefficient. To build the reduced ODE system, the same features of the linear case were used. Its reduced system was written with an explicit formulation and then implemented in `Matlab`. In the highly nonlinear case, the reduced system is numerically obtained as the ODE system can not be explicitly expressed. The third case study focused on a such general highly nonlinear transfer model, with material properties strongly dependent on the relative humidity field. To treat the nonlinearities, the Chebyshev–Gauss quadrature was employed to solve the integrals. Again, the accuracy of the approach has been demonstrated by representing accurately the physical phenomenon, with an absolute error of the order of $\mathcal{O}(10^{-4})$ comparing to the reference solution. A parametric study on the number of modes and the tolerance of the ODE solver has also been carried out. Moreover, when comparing the CPU time of the different approaches, the Crank–Nicolson is one hundred times longer than the Spectral method to compute the solution. These results are still encouraging for future work on the integration of the Spectral method to 2D problems and to the highly nonlinear coupled problem of heat and moisture transfer.

In addition, the *Part 2* [15] of this work aims at comparing the Spectral approach to the Proper Generalised Decomposition (PGD) method, recently applied in building physics [6].

Acknowledgments

The authors acknowledge the Brazilian Agencies CAPES of the Ministry of Education and CNPQ of the Ministry of Science, Technology and Innovation, for the financial support.

Nomenclature

	Latin letters	
c_m	moisture storage capacity	[kg/m^3/Pa]
d_m	moisture diffusion	[s]
g	liquid flux	[kg/m^2/s]
h_v	vapour convective transfer coefficient	[s/m]
k	permeability	[s]
L	length	[m]
P_c	capillary pressure	[Pa]
P_s	saturation pressure	[Pa]
P_v	vapour pressure	[Pa]
R_v	water gas constant	[J/kg/K]
T	temperature	[K]
	Greek letters	
ϕ	relative humidity	[−]
ρ	specific mass	[kg/m^3]
	Abbreviations	
ODE	Ordinary Differential Equation	
ROM	Reduced Order Model	

A. Dimensionless values

A.1. Case from Section 4.1

Problem (2.6) is considered with $g^\star_{l,\mathrm{L}} = g^\star_{l,\mathrm{R}} = 0$ and the dimensionless properties of the material are equal to $d^\star_m = 1$ and $c^\star_m = 8.6$. The reference time is $t^0 = 1$ h, thus the final simulation time is fixed to $\tau^\star = 120$. The Biot numbers are $\mathrm{Bi}_{v,\mathrm{L}} = 101.5$ and $\mathrm{Bi}_{v,\mathrm{R}} = 15.2$. The boundary conditions are expressed as:

$$u_{\mathrm{L}}(t^\star) = 1 + \frac{1}{2}\sin\left(\frac{2\pi\, t^\star}{24}\right) + \frac{1}{2}\sin\left(\frac{2\pi\, t^\star}{4}\right),$$
$$u_{\mathrm{R}}(t^\star) = 1 + \frac{4}{5}\sin\left(\frac{2\pi\, t^\star}{12}\right).$$

A.2. Case from Section 4.2

Simplification of the problem (2.6) are carried out, $g^\star_{l,\mathrm{L}} = g^\star_{l,\mathrm{R}} = 0$ and $\nu(u) = d^\star_m(u)/c^\star_m(u)$. In this way, the dimensionless system is then written as:

$$\frac{\partial u}{\partial t^\star} = \nu(u)\,\frac{\partial^2 u}{\partial x^{\star 2}}, \qquad t^\star > 0, \qquad x^\star \in \big[0,\,1\big], \tag{A.1a}$$

$$\frac{\partial u}{\partial x^\star} = \mathrm{Bi}_{v,\mathrm{L}} \cdot \Big(u - u_{\mathrm{L}}\,(t^\star) \Big), \qquad t^\star > 0, \qquad x^\star = 0, \tag{A.1b}$$

$$-\frac{\partial u}{\partial x^\star} = \mathrm{Bi}_{v,\mathrm{R}} \cdot \Big(u - u_{\mathrm{R}}\,(t^\star) \Big), \qquad t^\star > 0, \qquad x^\star = 1, \tag{A.1c}$$

$$u = 1, \qquad t^\star = 0, \qquad x^\star \in \big[0,\,1\big]. \tag{A.1d}$$

The reference time is $t^0 = 1\ \mathsf{h}$, thus the final simulation time is fixed to $\tau^\star = 72$. The Biot numbers are $\mathrm{Bi}_{v,\mathrm{L}} = 15.2$ and $\mathrm{Bi}_{v,\mathrm{R}} = 101.5$. The boundary conditions are expressed as:

$$u_{\mathrm{L}}(t^\star) = 1 + \frac{1}{2}\,\sin^2\left(\frac{2\pi\,t^\star}{90}\right),$$

$$u_{\mathrm{R}}(t^\star) = 1 + \frac{3}{5}\,\sin^2\left(\frac{2\pi\,t^\star}{48}\right).$$

and, the dimensionless property of the material is:

$$\nu\Big(u(x\,,t)\Big) = 1.1 \cdot 10^{-2} + 5 \cdot 10^{-2} \cdot u\,(x\,,t)\,.$$

A.3. Case from Section 5.1

Problem (2.6) is considered with $g^\star_{l,\mathrm{L}} = g^\star_{l,\mathrm{R}} = 0$. In this way, the dimensionless governing equations are then written as:

$$c^\star_m(u)\,\frac{\partial u}{\partial t^\star} = \frac{\partial}{\partial x^\star}\left(d^\star_m(u)\,\frac{\partial u}{\partial x^\star} \right), \qquad t^\star > 0, \qquad x^\star \in \big[0,\,1\big], \tag{A.2a}$$

$$d^\star_m(u)\,\frac{\partial u}{\partial x^\star} = \mathrm{Bi}_{v,\mathrm{L}} \cdot \Big(u - u_{\mathrm{L}}\,(t^\star) \Big), \qquad t^\star > 0, \qquad x^\star = 0, \tag{A.2b}$$

$$-d^\star_m(u)\,\frac{\partial u}{\partial x^\star} = \mathrm{Bi}_{v,\mathrm{R}} \cdot \Big(u - u_{\mathrm{R}}\,(t^\star) \Big), \qquad t^\star > 0, \qquad x^\star = 1, \tag{A.2c}$$

$$u = 1, \qquad t^\star = 0, \qquad x^\star \in \big[0,\,1\big]. \tag{A.2d}$$

in which, the dimensionless properties of the material are:

$$d^\star_m(u) = 1 + 0.91\,u + 600 \cdot \exp\Big[-10\,\big(u - 1.5 \big)^2 \Big],$$

$$c^\star_m(u) = 900 - 656\,u + 10^4 \cdot \exp\Big[-5\,\big(u - 1.5 \big)^2 \Big].$$

Simulations are performed for a total time of $\tau^\star = 120$. The ambient water vapour pressure at the boundaries are different from the previous case study. At the left boundary, u_{L} has a fast jump until the saturation state $u_{\mathrm{L}} = 2,\ \forall t \in \left[10,\, 40\right]$ and at the right boundary, $u_{\mathrm{R}}(t^\star) = 1 + 0.8 \sin\left(\dfrac{2\pi\, t^\star}{4}\right)$, with $\mathrm{Bi}_{v,\mathrm{L}} = 101.5$ and $\mathrm{Bi}_{v,\mathrm{R}} = 15.2$.

References

[1] K. Abahri, R. Bennacer, and R. Belarbi. Sensitivity analyses of convective and diffusive driving potentials on combined heat air and mass transfer in hygroscopic materials. *Numerical Heat Transfer, Part A: Applications*, 69(10):1079–1091, 2016. 6

[2] M. Abuku, H. Janssen, and S. Roels. Impact of wind-driven rain on historic brick wall buildings in a moderately cold and humid climate: Numerical analyses of mould growth risk, indoor climate and energy consumption. *Energy and Buildings*, 41(1):101–110, 2009. 5

[3] A. H. Al-Mohy and N. J. Higham. A New Scaling and Squaring Algorithm for the Matrix Exponential. *SIAM J. Matrix Anal. Appl.*, 31(3):970–989, 2010. 12

[4] A. H. Al-Mohy and N. J. Higham. Computing the Action of the Matrix Exponential, with an Application to Exponential Integrators. *SIAM J. Sci. Comput.*, 33(2):488–511, 2011. 12, 13

[5] B. Bauklimatik Dresden. Simulation program for the calculation of coupled heat, moisture, air, pollutant, and salt transport. *http://www.bauklimatik-dresden.de/delphin/index.php?aLa=en*, 2011. 5

[6] J. Berger, N. Mendes, S. Guernouti, M. Woloszyn, and F. Chinesta. Review of Reduced Order Models for Heat and Moisture Transfer in Building Physics with Emphasis in PGD Approaches. *Archives of Computational Methods in Engineering*, pages 1–13, 2016. 6, 34

[7] J. P. Boyd. *Chebyshev and Fourier Spectral Methods*. New York, 2nd edition, 2000. 8

[8] D. M. Burch. An Analysis of Moisture Accumulation in Walls Subjected to Hot and Humid Climates. *ASHRAE Transactions*, 93(16):429–439, 1993. 5

[9] C. Canuto, M. Y. Hussaini, A. Quarteroni, and T. A. Zang. *Spectral Methods Fundamentals in Single Domains*. Scientific Computation. Springer-Verlag Berlin Heidelberg, 2006. 11

[10] S. M. Cox and P. C. Matthews. Exponential Time Differencing for Stiff Systems. *J. Comp. Phys.*, 176(2):430–455, 2002. 13

[11] A. Dalgliesh, S. Cornick, W. Maref, and P. Mukhopadhyaya. Hygrothermal Performance of Building Envelopes: Uses for 2D and 1D simulation. In *10th Conference on Building Science and Technology*, Ottawa, Canada, 2005. NRC Publication Archive. 5

[12] G. H. Dos Santos and N. Mendes. Simultaneous heat and moisture transfer in soils combined with building simulation. *Energy and Buildings*, 38(4):303–314, 2006. 5

[13] T. A. Driscoll, N. Hale, and L. N. Trefethen. Chebfun Guide. *Pafnuty Publications*, Oxford, 2014. 15, 28

[14] I. Fraunhofer. Wufi. *http://www.hoki.ibp.fhg.de/wufi/wufi_frame_e.html*, 2005. 5

[15] S. Gasparin, J. Berger, D. Dutykh, and N. Mendes. Spectral Methods - Part 2: A comparative study of reduced order models for moisture diffusion problems in Building Physics. *In preparation*, 2017. 34

[16] S. Gasparin, J. Berger, D. Dutykh, and N. Mendes. Stable explicit schemes for simulation of nonlinear moisture transfer in porous materials. *J. Building Perf. Simul.*, pages 1–21, 2017. 8, 14, 28

[17] W. Gautschi. *Orthogonal Polynomials: Computation and Approximation*. Oxford University Press, Oxford, UK, 2004. 9

[18] D. W. Hahn and M. N. Özisik. *Heat conduction*. Wiley-Interscience, New York, 3 edition, 2012. 16

[19] H. Janssen. Simulation efficiency and accuracy of different moisture transfer potentials. *J. Building Perf. Simul.*, 7(5):379–389, 2014. 5, 28

[20] H. Janssen, B. Blocken, and J. Carmeliet. Conservative modelling of the moisture and heat transfer in building components under atmospheric excitation. *Int. J. Heat Mass Transfer*, 50(5-6):1128–1140, 2007. 5

[21] C. S. Kenney and A. J. Laub. A Schur-Fréchet Algorithm for Computing the Logarithm and Exponential of a Matrix. *SIAM J. Matrix Anal. Appl.*, 19(3):640–663, 1998. 12

[22] D. J. Lucia, P. S. Beran, and W. A. Silva. Reduced-order modeling: new approaches for computational physics. *Progress in Aerospace Sciences*, 40(1-2):51–117, 2004. 5

[23] A. V. Luikov. *Heat and mass transfer in capillary-porous bodies*. Pergamon Press, New York, 1966. 6

[24] N. Mendes. *Models for prediction of heat and moisture transfer through porous building elements*. PhD thesis, Federal University of Santa Catarina - UFSC, 1997. 5

[25] N. Mendes, M. Chhay, J. Berger, and D. Dutykh. *Numerical methods for diffusion phenomena in building physics*. PUCPRess, Curitiba, Parana, 2017. 9

[26] N. Mendes and P. C. Philippi. A method for predicting heat and moisture transfer through multilayered walls based on temperature and moisture content gradients. *Int. J. Heat Mass Transfer*, 48(1):37–51, 2005. 5

[27] N. Mendes, I. Ridley, R. Lamberts, P. C. Philippi, and K. Budag. Umidus: A PC program for the Prediction of Heat and Mass Transfer in Porous Building Elements. In *IBPSA 99*, pages 277–283, Japan, 1999. International Conference on Building Performance Simulation. 5

[28] C. Moler and C. Van Loan. Nineteen Dubious Ways to Compute the Exponential of a Matrix, Twenty-Five Years Later. *SIAM Review*, 45(1):3–49, 2003. 12

[29] L. H. Mortensen, M. Woloszyn, C. Rode, and R. Peuhkuri. Investigation of Microclimate by CFD Modeling of Moisture Interactions between Air and Constructions. *J. Building Phys.*, 30(4):279–315, 2007. 5

[30] R. Peyret. *Spectral methods for incompressible viscous flow*. Springer-Verlag, New York, 2002. 9, 10

[31] PUCPR. Domus. *http://www.domus.pucpr.br/*, (Pontifical Catholic University of Parana), 2016. 5

[32] C. Rode and K. Grau. Whole Building Hygrothermal Simulation Model. *ASHRAE Transactions*, 109(1):572–582, 2003. 5

[33] S. Rouchier, M. Woloszyn, G. Foray, and J.-J. Roux. Influence of concrete fracture on the rain infiltration and thermal performance of building facades. *Int. J. Heat Mass Transfer*, 61:340–352, 2013. 5

[34] L. F. Shampine and M. W. Reichelt. The MATLAB ODE Suite. *SIAM J. Sci. Comput.*, 18:1–22, 1997. 25

[35] H.-J. Steeman, M. Van Belleghem, A. Janssens, and M. De Paepe. Coupled simulation of heat and moisture transport in air and porous materials for the assessment of moisture related damage. *Building and Environment*, 44(10):2176–2184, 2009. 5

[36] L. N. Trefethen. *Finite Difference and Spectral Methods for Ordinary and Partial Differential Equations*. Unpublished, Ithaca, NY, USA, 1996. 8

[37] M. Woloszyn and C. Rode. Tools for performance simulation of heat, air and moisture conditions of whole buildings. *Building Simulation*, 1(1):5–24, 2008. 5

S. Gasparin: LAMA, UMR 5127 CNRS, Université Savoie Mont Blanc, Campus Scientifique, F-73376 Le Bourget-du-Lac Cedex, France and Thermal Systems Laboratory, Mechanical Engineering Graduate Program, Pontifical Catholic University of Paraná, Rua Imaculada Conceição, 1155, CEP: 80215-901, Curitiba – Paraná, Brazil
E-mail address: suelengasparin@hotmail.com
URL: https://www.researchgate.net/profile/Suelen_Gasparin/

J. Berger: LOCIE, UMR 5271 CNRS, Université Savoie Mont Blanc, Campus Scientifique, F-73376 Le Bourget-du-Lac Cedex, France
E-mail address: Berger.Julien@univ-smb.fr
URL: https://www.researchgate.net/profile/Julien_Berger3/

D. Dutykh: LAMA, UMR 5127 CNRS, Université Savoie Mont Blanc, Campus Scientifique, F-73376 Le Bourget-du-Lac Cedex, France
E-mail address: Denys.Dutykh@univ-smb.fr
URL: http://www.denys-dutykh.com/

N. Mendes: Thermal Systems Laboratory, Mechanical Engineering Graduate Program, Pontifical Catholic University of Paraná, Rua Imaculada Conceição, 1155, CEP: 80215-901, Curitiba – Paraná, Brazil
E-mail address: Nathan.Mendes@pucpr.edu.br
URL: https://www.researchgate.net/profile/Nathan_Mendes/